

A&A manuscript no.
(will be inserted by hand later)

Your thesaurus codes are:
03(11.01.2; 11.06.2; 11.14.1; 11.16.1)

ASTRONOMY
AND
ASTROPHYSICS

October 27, 1999

The optical properties of low redshift radio galaxies

Federica Govoni^{1,3}, Renato Falomo¹, Giovanni Fasano¹ and Riccardo Scarpa²

¹ Osservatorio Astronomico di Padova, Vicolo dell'Osservatorio 5, I-35122 Padova, Italy

² Space Telescope Science Institute, 3700 San Martin Drive, Baltimore, MD 21218, U.S.A

³ Dipartimento di Astronomia dell'Università di Bologna, Via Ranzani 1, I-40127 Bologna, Italy.

Received; Accepted

Abstract. We present morphological and photometric properties of 79 low redshift ($z \leq 0.12$) radio galaxies extracted from two radio flux limited samples of radio sources.

All objects are imaged in the R band and for a sub-sample we have also obtained B band images. The sample includes sources of both FRI and FRII radio morphological type. Through the decomposition of the luminosity profiles and the analysis of the structural profiles (ellipticity, PA, c4) of the galaxies we are able to characterize in detail the optical properties of the radio galaxies.

It is found that most of host galaxies are luminous bulge dominated systems similar to normal giant ellipticals. Some cases of additional disk components are found whose spheroid-to-disk luminosity ratio is similar to that found in S0 galaxies.

The average absolute magnitude is $\langle M_{HOST}(tot) \rangle = -24.0$ with a clear trend for FRI sources to be ~ 0.5 mag brighter than FRII galaxies.

In about 40% of the objects observed we find an excess of light in the nucleus that is attributed to the presence of a nuclear point source whose luminosity is on average ~ 1 -2% of the total flux of the host galaxy. The luminosity of these nuclear point sources appears correlated with the core radio power of the galaxies.

Radio galaxies follow the same $\mu_e - R_e$ relationship as normal elliptical galaxies.

The distribution of ellipticity, the amount of twisting and shape of isophotes (*boxy*, *disky*) do not differ significantly from other ellipticals. The evidence for recent interactions is therefore rather modest.

Finally on average radio galaxies are bluer and have a color dispersion larger than normal elliptical galaxies, and the average color gradient in radio galaxies appears slightly steeper than in normal ellipticals.

These results support a scenario where radio emission is weakly related with the overall properties and/or the

activity have negligible effects on the global characteristics of the host galaxy.

Key words: Galaxies: active; Galaxies: fundamental parameters; Galaxies: nuclei; Galaxies: photometry

1. Introduction

Radio galaxies are the nearest kind of radio-loud active galactic nuclei (AGN). These objects can be detected and studied in the local universe as well as at very large distances (Pentericci et al. 1999).

Advances in radio astronomy have produced a wealth of data and information on the properties of the radio emitting regions at various physical scales. A simple but important morphological classification of extended radio sources was made by Fanaroff & Riley (1974), who pointed out that low-power sources tend to be brighter close to their nuclei whereas high-power ones are brighter at their outer extremities. Although on the kpc scale radio galaxies of high and low luminosity have quite different radio morphologies, VLBI observations suggest that both FR I and II sources have similar relativistic flows on parsec scale (Giovannini et al. 1994).

In the optical band photometric studies of radio galaxies have been carried out by various authors for different samples of radio galaxies (Hine & Longair 1979; Longair & Seldner 1979; Lilly & Prestage 1987; Prestage & Peacock 1988; Owen & Laing 1989; Smith & Heckman 1989a,b; Owen & White 1991; Gonzalez-Serrano et al. 1993; de Juan et al. 1994; Colina & de Juan 1995; Ledlow & Owen 1995).

Optical studies have been focused either on the morphological properties of host galaxies or on the properties of their close environment. Moreover many of these investigations have considered specific kinds of sources: powerful radio galaxies (Lilly & Prestage 1987, Smith & Heckman 1989b); FRI radio sources (Colina & de Juan 1995); radio galaxies in clusters, mostly FRI sources (Ledlow & Owen 1995).

Send offprint requests to: R. Falomo (falomo@pd.astro.it)

Based on observations collected at the European Southern Observatory, La Silla, Chile.

Based on observations collected at the Nordic Optical Telescope, La Palma.

Depending on the quality of data and the kind of analysis performed it was possible to extract both photometric and morphological properties of galaxies: total optical luminosity, overall morphology, scale length (effective radius), ellipticity, isophote twisting, presence of nuclear components, centering of isophotes, isophotal shape, presence of close companions and statistics about disturbed morphology.

Usually, host galaxies of radio sources are found to be luminous and large ellipticals often interacting with close companion galaxies. Distortion of the isophotes (displacement of the center and twisting), excesses over a de Vaucouleurs law, and the presence of nearby companions have been reported in an high fraction of FRI galaxies (Colina & de Juan 1995) and is assumed to be related with strong interactions/collisions between galaxies. Deviation of isophotes from pure ellipses were reported by Bender et al. (1987) and interpreted as an indication of recent merging. Smith & Heckman (1989b), looking at a sample of 72 powerful radio galaxies (at 178 MHz $P_{178} \geq 5 \times 10^{24}$ Watt/Hz), concluded that galaxy interactions/mergers play an important role in the powerful radio galaxy phenomenon. They found that over 50% of the sample galaxies exhibited peculiar optical morphologies such as shells, tidal bridges, and distorted isophotes.

The scenario which is emerging from the above mentioned studies is mainly focused on the connection between the radio activity phenomenon and the occurrence of close encounters and merging events in different environments. In particular, galaxies hosting FR II radio sources could result from interactions, in relatively poor environments, involving at least one gas-rich, dynamically cold galaxy (i.e. a disk galaxy). Instead, gravitational interactions and merging in richer environments, involving early-type galaxies alone, could give rise to FRI radio sources (see e.g. Colina & Perez-Fournon 1990).

In the light of this scenario, an important question that should be addressed is whether the ambient medium can trigger the radio emission. Fanti (1984), was the first to suggest that the probability of radio emission from elliptical galaxies does not depend on their location inside or outside the cluster. This was confirmed by a study on a large sample of radio galaxies by Ledlow & Owen (1995), who also conclude that the properties of radio sources do not depend on the optical richness of the cluster within which the galaxy resides. This would imply that the probability for a galaxy to form a radio source is not dependent on the environment. The probability of detecting radio emission from an elliptical galaxy is mostly dependent on the optical luminosity. Ledlow & Owen (1995) have also compared the optical properties of a sample of 265 FRI radio galaxies in rich clusters with a sample of radio-quiet galaxies selected from the same environment. They found that the local density of nearby companions and the frequency of morphological peculiarities or tidal interactions are not significantly different between the radio-loud and

radio-quiet samples. Therefore the link between radio activity and galaxy interaction is not yet clear and the point must be further investigated.

Concerning the integrated optical properties, galaxies associated with FRI radio morphologies seem intrinsically brighter and larger than those hosting FR II sources (Owen & Laing 1989). In particular, according to Prestage & Peacock (1988), FRIs are associated with giant ellipticals similar to first ranked galaxies and can be found in the cores of rich clusters, while FR IIs are identified with galaxies of lower luminosity and are usually found in poorer clusters. At $z \sim 0.5$ the situation changes and both FRI and FR II sources seem to lie in similar rich environments (Hill & Lilly 1991).

Another important point concerns the very nature of galaxies hosting radio sources. It is commonly assumed that these galaxies are giant ellipticals or bulge-dominated systems. However, their brightness profiles often exhibit marked deviations from a pure de Vaucouleurs ($r^{1/4}$) law, suggesting the presence of additional components in both the nuclear and the external regions. These may be ascribed to unresolved nuclear sources, small inner disks, extended halos or underlying disks.

The presence of nuclear point sources in the cores of radio galaxies was first investigated by Smith & Heckman (1989b) who reported that the light profiles of radio galaxies are consistent with an $r^{1/4}$ law with, in some cases (18 %), an additional point source at the nucleus.

The study of the galaxies hosting radio sources and of the relation between optical and radio properties of galaxies is an important tool for understanding the nature of radio galaxies. In order to elucidate some of the above mentioned points we have therefore undertaken an optical study of a large sample (79 sources) of low-redshift ($z \leq 0.12$) radio galaxies. At this redshift limit we are able to investigate in detail galaxy properties using ground-based telescopes data. Our sample includes both FRI and FR II with radio power in the range $\sim 1.8 \times 10^{23} - 3.1 \times 10^{26}$ Watt/Hz at 2700 MHz.

We used R band imaging to derive morphological and photometric properties of the radio galaxies in the sample. These include structural (ellipticity, isophote twisting, Fourier coefficients, etc.) and integrated observed properties (isophotal and total magnitude, effective radius, etc.). In particular we investigated the shape of the luminosity profile and determined the contribution of the (unresolved) nuclear source.

Details on the observations are given in:

- 1) Fasano et al. 1996 (Paper I), where we present the results for a subset of 29 radio sources of the sample for which imaging in both R and B band is available.
- 2) Govoni et al. 1999 (Paper II), where we present the observational results from R band imaging of the remaining galaxies (50 objects) in the sample.

The plan of this paper is the following: in Sect. 2 we describe the optical data and the radio morphologies of the

Table 1. Radio properties

IAU name (1)	z (2)	Smp. (3)	FR-class (4)	Ref. ^a (5)	S_{408MHz} (Jy) (6)	$S_{2.7GHz}$ (Jy) (7)	$S(core)_{4.8GHz}$ (Jy) (8)
0005 – 199	0.121	EK	I	2	2.08	0.45	0.014
0013 – 316	0.107	EK	I	2	1.36	0.24	0.005
0023 – 333	0.05	EK	I	2	4.09	0.73	0.010
0034 – 014	0.073	WP	I/II	1	9.74	2.56	0.299
0055 – 016	0.045	WP	I	1	10.9	3.46	0.093
0123 – 016	0.018	WP	I/II	1	16.4	3.29	0.100
0131 – 367	0.03	WP	II	1,2,3	...	5.6	0.038
0229 – 208	0.089	EK	I	2	2.52	0.75	0.093
0247 – 207	0.087	EK	I	2	3.3	0.54	0.023
0255 + 058	0.023	WP	I	1	16.2	3.3	0.039
0257 – 398	0.066	EK	II	2	2.57	0.61	<0.004
0307 – 305	0.066	EK	II	2	1.98	0.64	0.003
0312 – 343	0.067	EK	I	2	0.94	0.25	0.025
0325 + 023	0.03	WP	II	1	10.90	3.18	0.159
0332 – 391	0.063	EK	I	2,3	4.2	0.94	0.013
0344 – 345	0.053	EK	I	2,3	7.6	2.08	0.040
0349 – 278	0.066	EK	II	1,2	13.7	3.24	0.016
0427 – 539	0.038	WP	I	1	14.6	3.84	0.057
0430 + 052	0.033	WP	I	1	6.08	3.0	3.458
0434 – 225	0.069	EK	I	2	2.26	0.66	0.009
0446 – 206	0.073	EK	I	2	2.3	0.38	0.009
0449 – 175	0.031	EK	I	2	1.85	0.64	0.010
0452 – 190	0.039	EK	I	2	0.66	0.25	0.025
0453 – 206	0.035	WP	I/II	1	11.3	2.79	0.04
0511 – 305	0.058	EK	II	2,3	7.8	1.66	0.010
0533 – 377	0.096	EK	I	2	0.96	0.3	0.013
0546 – 329	0.037	EK	I	2,3	2.89	0.43	0.032
0548 – 317	0.034	EK	II	2	2.3	0.68	<0.006
0620 – 526	0.051	WP	I	1	9.3	2.1	0.260
0625 – 354	0.055	WP	I	2	7.83	2.9	0.600
0625 – 536	0.054	WP	II	1	20.2	3.7	0.042
0634 – 205	0.056	EK	I/II	2	22.8	4.5	0.012
0712 – 349	0.044	EK	I	2	0.74	0.21	0.025
0718 – 340	0.029	EK	I/II	2	4.1	1.36	0.030
0806 – 103	0.11	WP	II	1	13.7	2.49	0.055
0915 – 118	0.054	WP	I	1	132.0	23.5	0.217
0940 – 304	0.038	EK	I	2	0.68	0.29	0.047
0945 + 076	0.086	WP	II	1	22.1	4.3	0.032
1002 – 320	0.089	EK	I	2,3	2.66	0.4	<0.005
1043 – 290	0.06	EK	I	2	0.88	0.39	0.055
1053 – 282	0.061	EK	I	2	3.51	1.28	0.115
1056 – 360	0.07	EK	I/II	2,3	4.09	0.96	0.050
1107 – 372	0.01	EK	I	2	0.96	0.41	0.010
1123 – 351	0.032	EK	I	2	6.61	1.43	0.070
1251 – 122	0.015	WP	I	1	14.7	4.5	0.088
1251 – 289	0.057	EK	I	2	4.22	0.48	<0.010
1257 – 253	0.065	EK	I	2	1.5	0.45	0.016
1258 – 321	0.017	EK	I	2	2.99	0.92	0.100
1318 – 434	0.011	WP	I	1	...	3.09	0.58
1323 – 271	0.044	EK	U	2	3.75	0.94	0.015
1333 – 337	0.013	WP	I/II	1,2,3	34.0	10.06	0.297
1344 – 241	0.02	EK	I	2	2.38	0.39	<0.004
1354 – 251	0.038	EK	I	2	1.08	0.43	0.005

Table 1 (continued). Radio properties

IAU name (1)	z (2)	Smp. (3)	FR-class (4)	Ref. ^a (5)	S_{408MHz} (Jy) (6)	$S_{2.7GHz}$ (Jy) (7)	$S(core)_{4.8GHz}$ (Jy) (8)
1400 – 337	0.014	EK	I	2	6.5	0.46	0.015
1404 – 267	0.022	EK	I?	2	1.09	0.5	0.280
1514 + 072	0.035	WP	I	1	25.2	2.2	0.391
1521 – 300	0.02	EK	I?	2	0.26	0.31	0.160
1637 – 771	0.041	WP	II	1,3	11.4	3.77	0.184
1717 – 009	0.031	WP	II	1	138.0	33.8	0.117
1733 – 565	0.098	WP	II	1	13.0	5.2	0.68
1928 – 340	0.098	EK	I	2	3.52	0.36	0.021
1929 – 397	0.073	EK	II	2	6.41	1.54	0.014
1949 + 023	0.059	WP	II	1	13.6	3.68	0.01
1954 – 552	0.058	WP	I	1,3	14.0	3.74	0.050
2013 – 308	0.088	EK	I	2,3	2.47	0.50	0.010
2031 – 359	0.088	EK	I	2	4.4	0.93	0.012
2040 – 267	0.041	EK	II	2	5.44	1.56	0.032
2058 – 282	0.039	WP	I/II	1	15.9	3.10	0.063
2059 – 311	0.039	EK	I	2	0.67	0.24	0.018
2104 – 256	0.038	WP	I/II	1	31.0	7.3	0.058
2128 – 388	0.018	EK	I	2	1.79	0.65	0.020
2158 – 380	0.034	EK	II	2,3	4.12	1.01	0.005
2209 – 255	0.063	EK	I?	2	0.5	0.26	0.050
2221 – 023	0.057	WP	II	1	17.5	3.46	0.086
2225 – 308	0.056	EK	I	2,3	2.07	0.55	0.030
2236 – 176	0.07	EK	I	2	4.31	1.06	0.010
2333 – 327	0.052	EK	II	2	0.67	0.23	0.012
2350 – 375	0.116	EK	I	2	0.76	0.25	0.004
2353 – 184	0.073	EK	I	2	2.05	0.49	0.010

^a References :

(1) Morganti et al. (1993) or Morganti et al. (1997);

(2) Ekers et al. (1989);

(3) Jones & Mc Adam (1992).

galaxies. In Sect. 3 we concentrate on the surface brightness profiles and in particular on the decomposition of the luminosity profiles. In Sect. 4 we describe the global properties of the galaxies (absolute magnitudes, effective radius, $\mu_e - R_e$ relation, and colors). In Sect. 5 we discuss the structural and morphological properties of the galaxies (ellipticity and isophote shape). In Sect. 6 we describe some signatures of interactions between galaxies (displacement of isophote and twisting). Finally, in Sect. 7 we summarize the results and draw the main conclusions of the work.

Throughout this paper we assume $H_0=50 \text{ km sec}^{-1} \text{ Mpc}^{-1}$ and $q_0=0$.

2. Optical and radio data

We have collected images in the Cousins R band for 79 radio galaxies at low redshift, belonging to a sample of 95 objects.

This sample is composed of radio galaxies extracted from two complete surveys of radio sources: The first one is the 2.7-GHz 2-Jy all-sky survey of radio sources with $S(2.7\text{GHz}) > 2\text{Jy}$ by Wall & Peacock (1985, hereafter WP), and the second one is the survey from Ekers et al. (1989, hereafter EK). The selection criteria of our sample are described in Paper I.

Detailed surface photometry and quantitative morphological analysis were performed using the AIAP package (Fasano 1990). Due to its high degree of interactivity, the AIAP software turns out to be particularly suitable for analyzing the morphology of galaxies embedded in high density regions, such as rich cluster or compact galaxy groups. The observational details and data reduction are described in Paper I and Paper II.

For each object we have also determined the shape of the point spread function (PSF) combining the radial brightness profiles of several stars of different magnitude

in each CCD frame. This allowed us to properly determine the PSF both in the center and in the wings.

For each object we report in Table 1 the object name, the redshift, and the parent sample (column 1, 2, and 3), together with radio data information (column 4, 5, 6, 7 and 8).

Concerning the radio data, most of the radio images of the objects belonging to the WP sample were obtained by Morganti et al. (1993) with the Very Large Array (VLA) and the Australia Telescope Compact Array (ATCA), while VLA radio images are available for most of the objects belonging to the EK sample.

Sources are classified according to the Fanaroff and Riley (FR) scheme (Fanaroff & Riley, 1974). Simply stated, the FRI sources are dominated by emission from the compact core and jets. The radio lobes in these sources are generally diffuse, and fade with the distance from the central source. The FR II sources have the highest surface brightness in the hotspots at the outer extremes of the lobes.

The radio morphology classification, given in column 4 of Table 1 (FRI and FR II indicated as I and II respectively), is mainly taken on the basis of the published radio images. Obviously, to allow a reliable classification of these radio sources according to the FR scheme, require good radio images (not always available). Objects with transition properties or with an unclear classification are marked as I/II. We indicate with U one unresolved source. Finally, in the few case of objects with no available radio images we report the likely class (labeled with a question mark) based on the power-morphology relationship. For these cases we classified as FRI all radio sources with luminosity less than 2×10^{25} Watt/Hz at 178 MHz.

Columns 6, 7 and 8 contain the radio fluxes at 408 MHz, at 2.7 GHz, and the core radio flux at 4.8 GHz respectively. In some cases only upper limits of the core flux are available. For the sources belonging to the list of EK we have taken the radio flux from this reference, while for the remaining objects the radio fluxes were taken from WP at 2.7 GHz, from the PKS catalogue at 408 MHz, and from Morganti et al. (1993) for the radio core at 4.8 GHz.

The average radio power at 2700 MHz turns out to be 1.1×10^{25} Watt/Hz.

3. Surface brightness profiles

3.1. Decomposition of the luminosity profiles

To the first order, radial brightness profiles $I(r)$ of elliptical galaxies are well described by the de Vaucouleurs law (1948) $\mu \propto r^{1/4}$:

$$I(r) = I_0 \exp\{-7.67[(r/r_e)^{1/4} - 1]\},$$

where I_0 is the surface brightness at $r = 0$ and r_e is the effective radius. In the case of radio galaxies, however,

deviations from this law are rather common, in particular when looking at the core or at the outer faint regions (Smith & Heckman 1989b; Colina & de Juan 1995). These deviations may be described either using extra components (e.g. inner disks, exponential law) or adopting a more general law (e.g. the Sersic (1968) law $\mu \propto r^{1/n}$) to represent the profile.

For the aims of this work we used a standard $r^{1/4}$ law (which remains a good description for the main body of most ellipticals) plus, when required, a nuclear component described by a PSF and an exponential law to account for extra emission in the outer regions $\mu \propto r$:

$$I(r) = I_d \exp[-r/r_d],$$

where I_d and r_d are the surface brightness at $r = 0$ and the scale-length of the exponential component respectively. This decomposition of the luminosity profile enables us to identify the presence of other components and to quantify deviations from the $r^{1/4}$ law. Following this approach we fitted the observed brightness profiles of each galaxy using different strategies, from visual inspection of the overall residuals, to best fit with χ^2 minimization. Errors associated with the profiles were computed using the prescriptions given by Fasano & Bonoli (1990).

In Fig. 1 we show our best decomposition of the brightness profiles while in Table 2 we give all the relevant parameters of the fit. Columns 2, 3 and 5 contain the magnitudes of point source, bulge and exponential component (m_{ps} , $m_{r^{1/4}}$, m_{exp}), respectively. The effective radius of the bulge (r_e) and the radius of the disk (r_d) in arcsec are reported in columns 4 and 6. Column 7 gives the value of χ^2 for the best fit. We list the different components of the profiles for each object in column 8, while in column 9 we give additional notes.

For 19 galaxies the luminosity profile is fairly well fitted by a simple de Vaucouleurs law (R14). For 13 galaxies we were not able to represent the external part of the luminosity profile with a $r^{1/4}$ law only, because of the presence of large excesses over the extrapolation of the $r^{1/4}$ law. In these cases we found an acceptable fit by adding an exponential component (EXP) to the $r^{1/4}$ one. For 28 sources the luminosity profile shows an excess over the $r^{1/4}$ law in the central unresolved region of the galaxy. This excess can be satisfactory described by an additional point source (PS, modeled by the PSF). On the contrary, 11 galaxies show an evident flattening (ABS) with respect to the $r^{1/4}$ law in the inner part of the luminosity profile. In 4 objects we found both a point source in the nucleus and an external exponential component, while in other 4 sources there is both a deficit of light in the central region and an exponential component. We summarize in Table 3 the statistics of the components for the observed objects. We found that the frequency of the different components in the brightness profiles of radio galaxies is not dependent on the radio morphology.

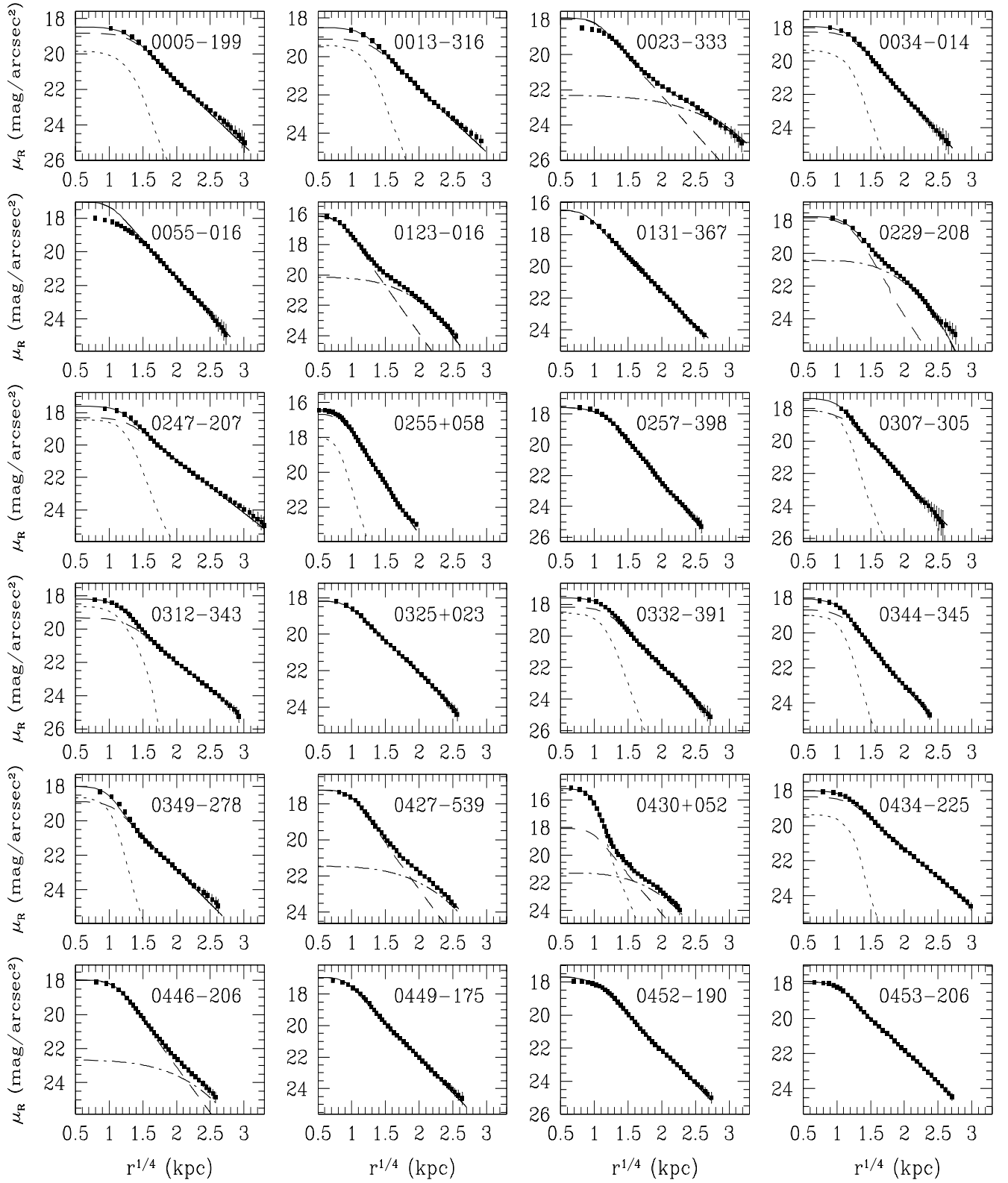


Fig. 1. Decomposition of the luminosity profile (filled dots in the figures) of the galaxies. These profiles are fitted with different components: point source (short dashed line), de Vaucouleurs law (long dashed line), exponential component (short dashed - long dashed line).

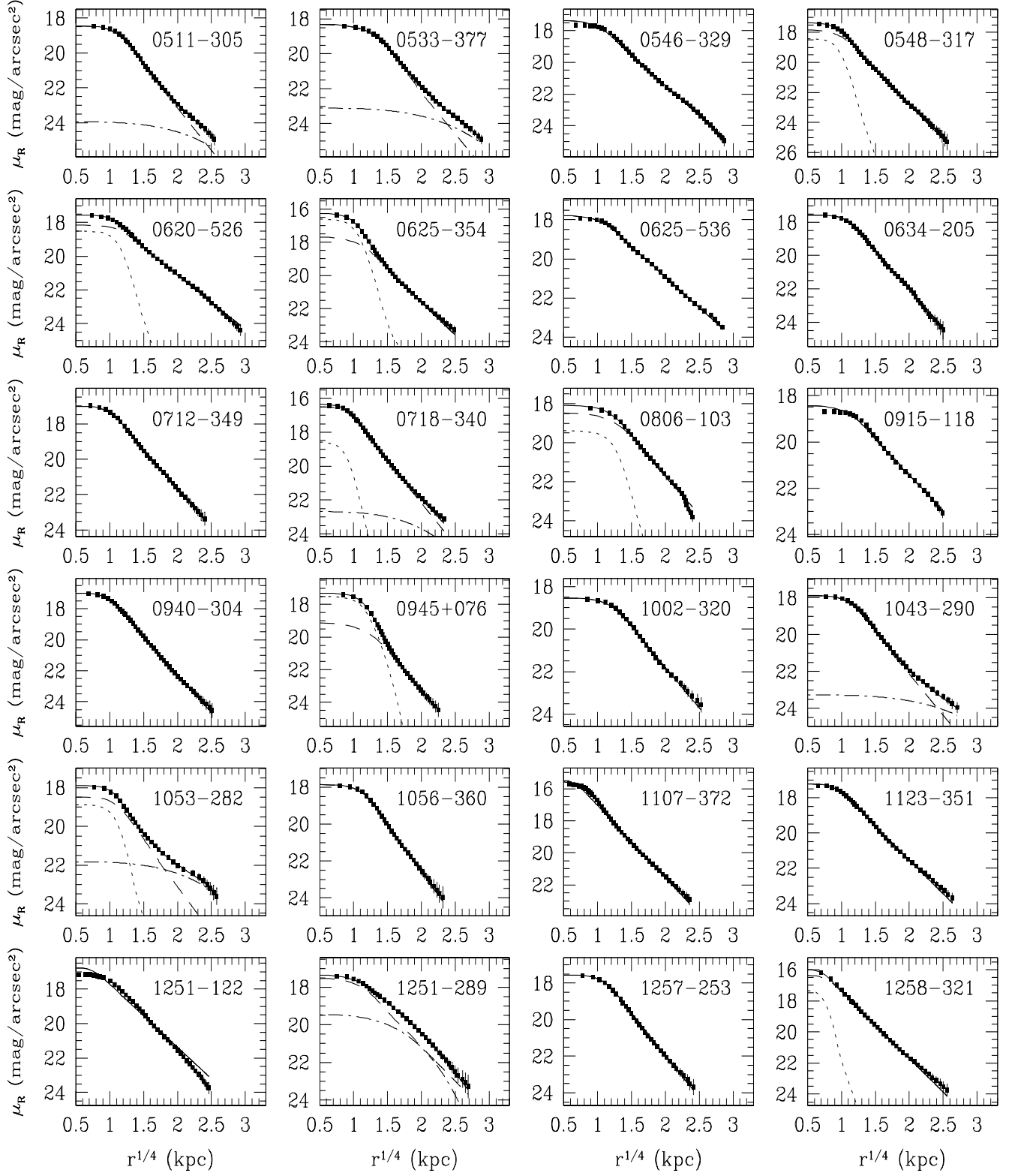


Fig. 1. Continued.

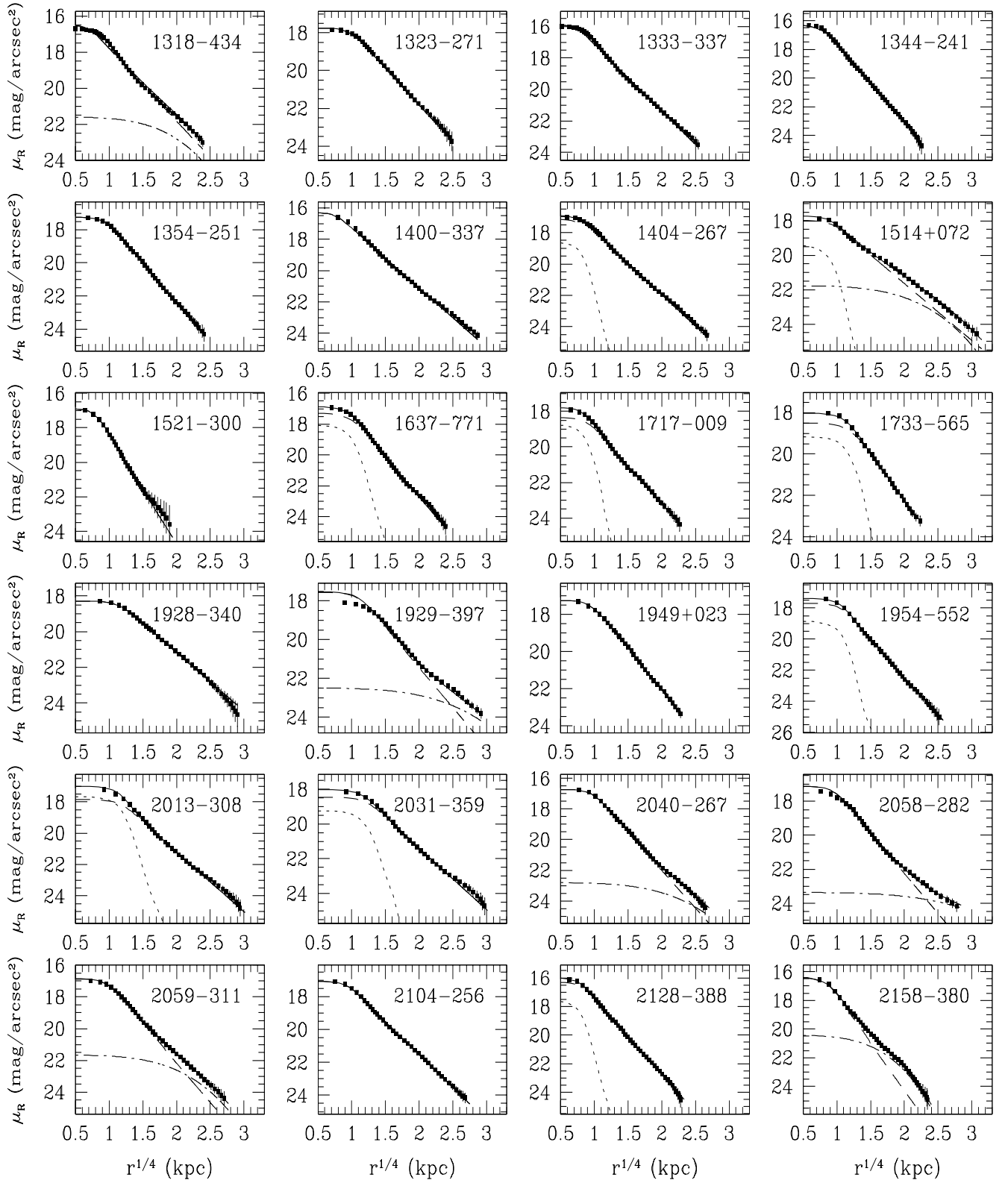


Fig. 1. Continued.

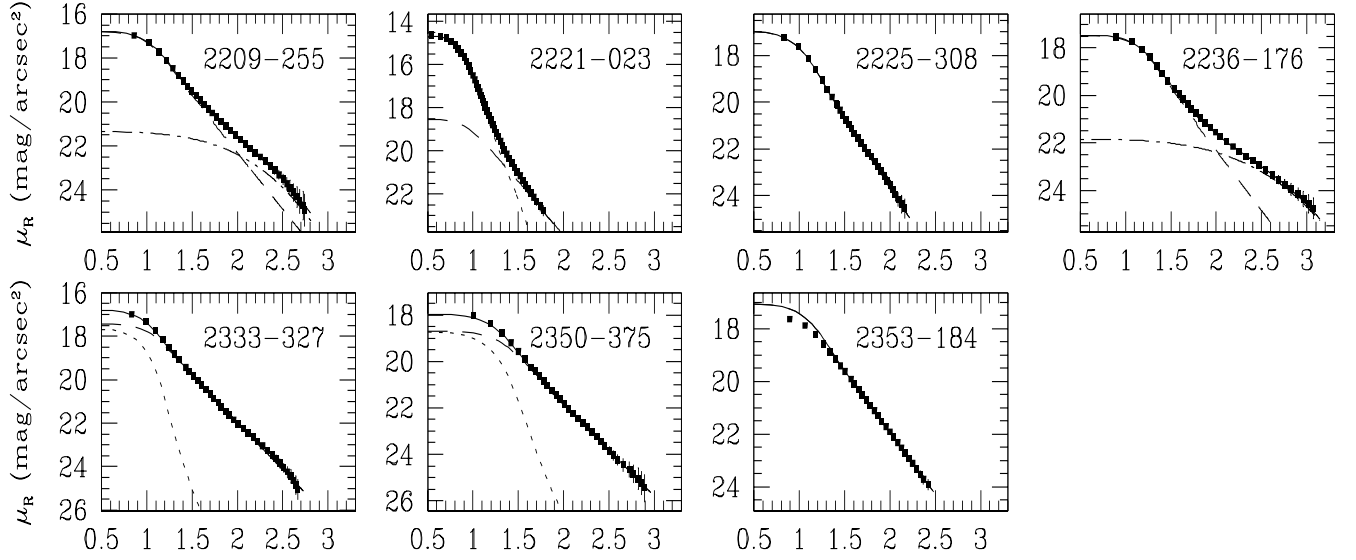


Fig. 1. Continued.

3.2. Nuclear sources

One interesting result of the present analysis of the luminosity profiles is that $\sim 40\%$ of objects in our sample suggests the presence of a nuclear point source. In particular in some cases (2221-023, 0430+052, 0625-354, 0945+076) this component is very prominent.

Most of the investigations of radio galaxies in the optical band have not tried to quantitatively determine the contributions of the nuclear emission. Only Smith & Heckman (1989b) in their study of 72 powerful radio galaxies have searched for point sources in the nuclei through image modeling. They used the results mainly to derive correction factors for the galaxy magnitudes. Excluding few peculiar sources (e.g. 3C371 which is a BL Lac object), they found point sources for 13 cases with magnitude M_V ranging from about -18 to -21 ($H_0 = 50$) and contributing to the total flux of the object by $\sim 10\%$ or less. This is consistent with the distribution of the nucleus/galaxy luminosity ratio we have found in our sample. This distribution is shown in Fig. 2 and peaks at $\text{Log}[\text{Nucl}/\text{Host}] \simeq -1.4$. Therefore in our sample of radio galaxies the average contribution of the nuclear source to the galaxy luminosity is $\sim 5\%$. Assuming that most of radio galaxies have a nuclear point source and that we are detecting only the brightest nuclei, the average ratio nucleus/host optical luminosity could be of the order of few percent.

Recent studies of radio galaxies using Hubble Space Telescope (HST) observations have confirmed the presence of bright optical nuclear unresolved components in galaxies hosting radio sources (Capetti & Celotti 1999; McLure et al. 1999; Chiaberge et al. 1999).

In BL Lac objects generally the nuclear source has a luminosity similar to that of the galaxy (Falomo et al. 1999), while in quasars the nucleus/host luminosity ratio is of the order of ~ 10 .

The distribution of the absolute magnitudes of the point sources is shown in Fig. 3a ($\langle M_{PS} \rangle = -20.4 \pm 1.3$; errors are given as the r.m.s throughout the paper), while Fig. 3b shows that the magnitude of the point source is not correlated with that of the host galaxy.

We derived an upper limit for the point source contribution in the galaxies where no point source is detected. This was done by adding a point source component at various levels and seeing when the contribution would become observable (see Table 5, column 8).

From Fig. 4, the radio core power appears weakly correlated with the luminosity of the point source. A linear correlation of the nuclear optical luminosity with the radio core was also recently reported for a sample of 33 FRI radio galaxies from 3CR catalogue observed with HST (Chiaberge et al. 1999).

Giovannini et al. (1988) found a relation between total radio power and core radio power ($\text{Log} P_{\text{core}} = 11.01 + 0.47 \text{Log} P_{\text{tot}}$) in a sample of 187 radio galaxies selected at low frequency. In Fig. 5 we plot the core radio power at 4800 MHz versus the total radio power at 408 MHz; our objects are divided according to the PS absolute magnitude.

The radio core power of our radio galaxies are systematically brighter with respect to this empirical relationship. This is probably due to the fact that our sample is biased toward high radio core power due to the high frequency (2700 MHz) at which the sample was selected. The scatter in the relation is attributed to the different

Table 2. Parameters of the radial profile fit

Name (1)	m_{ps} (2)	$m_{r,1/4}$ (3)	r_e (") (4)	m_{exp} (5)	r_d (") (6)	χ^2 (7)	Components ^a (8)	Notes (9)
0005 – 199	18.84	15.12	8.1	1.4	R14,PS	
0013 – 316	18.38	14.97	12.9	0.3	R14,PS	
0023 – 333	...	13.92	9.8	13.44	30.0	14.3	R14,ABS,EXP	halo
0034 – 014	18.11	14.68	6.3	0.2	R14,PS	
0055 – 016	...	13.07	9.7	R14,ABS	
0123 – 016	...	12.52	6.0	11.75	20.7	0.1	R14,EXP	disk
0131 – 367	...	12.15	16.7	1.5	R14,ABS	
0229 – 208	...	15.89	1.1	15.24	4.1	0.3	R14,EXP	possible disk
0247 – 207	17.02	13.62	17.1	0.9	R14,PS	
0255 + 058	17.35	13.57	8.4	0.7	R14,PS	
0257 – 398	...	14.54	3.7	1.0	R14	
0307 – 305	17.26	14.76	6.9	0.3	R14,PS	
0312 – 343	16.88	14.36	22.5	0.5	R14,PS	
0325 + 023	...	13.22	32.2	0.9	R14	
0332 – 391	17.09	14.17	8.6	0.2	R14,PS	
0344 – 345	17.73	14.98	8.2	0.1	R14,PS	
0349 – 278	18.33	15.23	10.9	2.6	R14,PS	
0427 – 539	...	13.71	6.7	13.94	17.1	0.2	R14,EXP	possible disk
0430 + 052	14.31	15.05	5.0	14.92	10.2	0.3	R14,PS,EXP	disk
0434 – 225	17.91	13.85	18.9	0.7	R14,PS	
0446 – 206	...	15.41	2.7	16.51	9.1	0.4	R14,EXP	halo
0449 – 175	...	12.77	13.6	1.5	R14,ABS	
0452 – 190	...	13.41	14.0	2.7	R14,ABS	
0453 – 206	...	12.9	26.5	0.2	R14	
0511 – 305	...	15.07	5.2	16.76	17.3	1.7	R14,EXP	halo
0533 – 377	...	15.27	3.5	16.32	13.3	0.5	R14,EXP	halo
0546 – 329	...	12.54	21.7	2.2	R14,ABS	
0548 – 317	17.08	13.67	11.0	0.2	R14,PS	
0620 – 526	16.88	12.94	30.2	0.3	R14,PS	
0625 – 354	15.77	13.95	12.2	0.4	R14,PS	
0625 – 536	...	12.97	33.1	0.2	R14,ABS	
0634 – 205	...	14.82	6.7	1.5	R14	
0712 – 349	...	13.98	10.1	0.7	R14	
0718 – 340	18.48	13.53	9.5	15.99	20.0	0.4	R14,PS,EXP	halo
0806 – 103	18.81	15.8	6.8	0.9	R14,PS	
0915 – 118	...	14.48	33.9	4.0	R14,ABS	
0940 – 304	...	13.69	7.7	1.0	R14	
0945 + 076	16.6	16.39	4.6	0.3	R14,PS	
1002 – 320	...	15.3	9.5	0.3	R14	
1043 – 290	...	14.38	7.0	15.56	30.0	0.6	R14,EXP	halo
1053 – 282	17.97	15.36	5.4	14.99	15.9	0.2	R14,PS,EXP	possible disk
1056 – 360	...	15.16	3.9	0.1	R14	
1107 – 372	...	10.16	40.4	8.1	R14,ABS	
1123 – 351	...	12.61	23.8	0.6	R14	small halo
1251 – 122	...	10.83	61.9	9.4	R14,ABS	
1251 – 289	...	13.47	16.2	13.91	5.9	0.1	R14,EXP	halo
1257 – 253	...	14.55	6.0	1.5	R14	
1258 – 321	16.65	11.35	28.3	0.5	R14,PS	small halo
1318 – 434	...	10.79	58.0	12.2	45.0	5.3	R14,ABS,EXP	halo
1323 – 271	...	13.62	17.3	0.7	R14	
1333 – 337	...	10.38	39.5	2.5	R14,ABS	
1344 – 241	...	12.71	9.5	0.4	R14	
1354 – 251	...	13.71	8.5	0.3	R14	

Table 2 (continued). Parameters of the radial profile fit

Name (1)	m_{ps} (2)	$m_{r^{1/4}}$ (3)	r_e (") (4)	m_{exp} (5)	r_d (") (6)	χ^2 (7)	Components ^a (8)	Notes (9)
1400 – 337	...	10.25	56.8	3.9	R14	
1404 – 267	17.85	12.09	29.0	0.7	R14,PS	
1514 + 072	18.73	12.51	39.2	13.12	25.0	3.2	R14,PS,EXP	possible disk
1521 – 300	...	14.06	5.4	0.6	R14	small halo
1637 – 771	17.18	14.12	6.0	0.6	R14,PS	
1717 – 009	18.42	14.53	16.4	0.6	R14,PS	
1733 – 565	18.74	16.09	5.4	0.2	R14,PS	
1928 – 340	...	14.58	15.1	0.1	R14	
1929 – 397	...	14.15	8.0	14.94	22.0	15.3	R14,ABS,EXP	halo
1949 + 023	...	14.86	6.9	0.1	R14	
1954 – 552	17.95	14.43	5.6	0.1	R14,PS	
2013 – 308	17.01	14.37	9.1	1.9	R14,PS	
2031 – 359	18.11	14.37	12.2	1.2	R14,PS	
2040 – 267	...	13.27	6.9	14.98	22.3	0.7	R14,EXP	halo
2058 – 282	...	13.53	8.6	14.52	68.9	5.2	R14,ABS,EXP	halo
2059 – 311	...	13.37	7.1	14.2	16.2	0.2	R14,EXP	possible disk
2104 – 256	...	12.84	17.1	0.6	R14	
2128 – 388	16.66	12.11	12.2	0.2	R14,PS	
2158 – 380	...	14.13	2.7	14.3	7.1	0.5	R14,EXP	disk
2209 – 255	...	14.26	3.8	14.8	9.1	0.1	R14,EXP	disk
2221 – 023	15.08	16.17	5.3	0.2	R14,PS	
2225 – 308	...	15.03	2.4	0.4	R14	
2236 – 176	...	14.55	3.6	14.34	15.1	0.1	R14,EXP	possible disk
2333 – 327	17.08	13.72	9.1	0.6	R14,PS	
2350 – 375	17.83	15.34	5.9	0.3	R14,PS	
2353 – 184	...	14.46	4.8	8.4	R14,ABS	

^a Decomposition of the brightness profiles:

R14 = de Vaucouleurs law; PS = unresolved component in the core of the source;

ABS = lack of light with respect to the de Vaucouleurs law in the center;

EXP = exponential component in the external region.

orientation of the sources with respect to the line of sight (Giovannini et al. 1988). Namely, sources pointing toward the observer have their radio core powers enhanced by Doppler boosting. Consistent with this view we note that the objects with more luminous optical point sources are located towards higher radio core power with respect to the objects for which no point source was detected (see Fig. 5).

3.3. Inner deficit of light

The luminosity profiles of 15 sources (5 cases are clearly evident in Fig. 1) show in the nuclear part a lack of light with respect to the de Vaucouleurs fit. This could be ascribed either to a substantial deviation from isothermal distribution of stars or to significant diffuse dust absorption. Wise & Silva (1997) examined the effects of dust on the central optical properties of elliptical galaxies. They found that smoothly distributed dust will significantly

suppress the surface brightness of the central region of ellipticals without being clearly visible in direct images. However this interpretation would imply a clear signature in the color profiles, which is not observed. On the other hand the presence of dust in the central regions of radio galaxies is often detected from HST images (Chiaberge et al. 1999; Kleijn et al. 1999) as dust lanes or dusty-disks. These features are, however, in general confined in a region of about 1 kpc and are therefore undetectable in ground based observations. From our images only a couple of galaxies show clear presence of dust features (see Paper I and Paper II for details).

3.4. External light excess

A significant fraction of radio galaxies in our sample ($\sim 25\%$) exhibit an excess over the $r^{1/4}$ fit for radii $r \geq r_e$. Similar light excesses have been reported by Colina & de Juan (1995) for most of the FRI radio galaxies in their

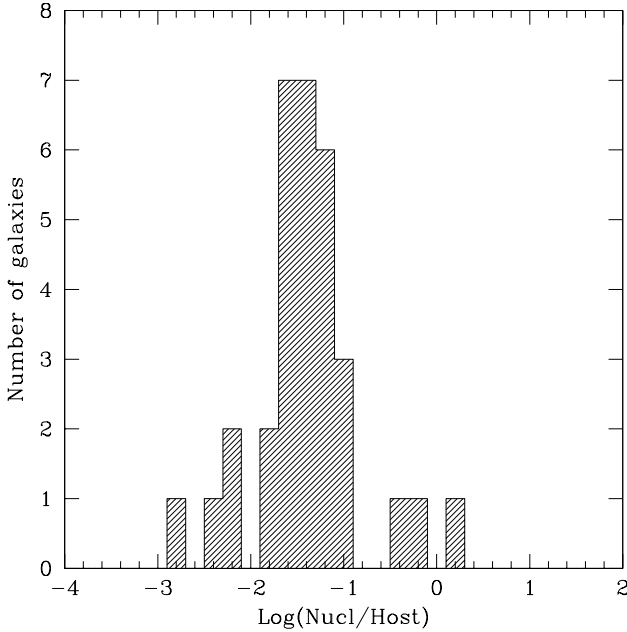
Table 3. Statistic of galaxy components

	R14	R14,PS	R14,PS,EXP	R14,ABS	R14,ABS,EXP	R14,EXP
All						
N. of objects	19	28	4	11	4	13
% of Objects	24%	35.5%	5%	14%	5%	16.5%
FRI						
N. of objects	10	16	3	8	2	8
% of objects	21.5%	34%	6%	17%	4.5%	17%
FRII						
N. of objects	3	10	0	2	1	3
% of objects	16%	52.5%	0%	10.5%	5%	16%

R14 : de Vaucouleurs law; PS : an unresolved component in the core of the source;

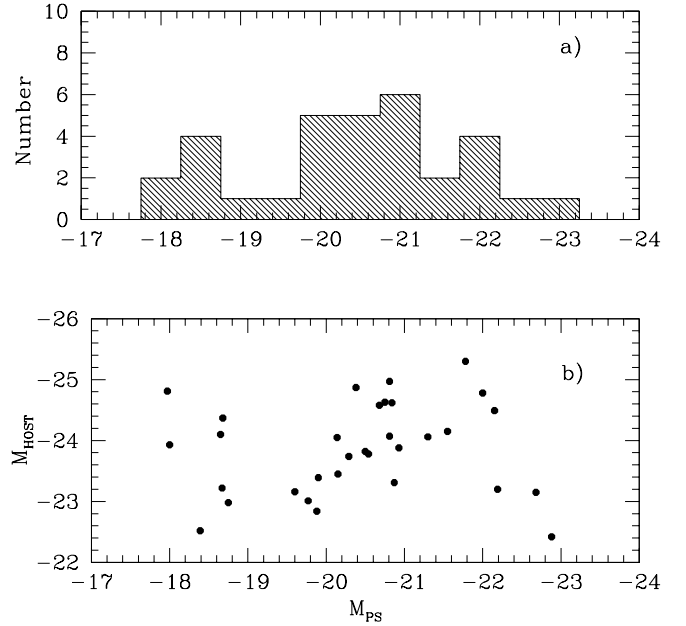
ABS : a lack of light with respect to the de Vaucouleurs law in the center;

EXP : an exponential component in the external region.

**Fig. 2.** Distribution of the nucleus/galaxy luminosity ratio ($\text{Log}[Nuc/Host]$) in our sample.

sample, and ascribed to the effects of galaxy interactions. While this interpretation could apply to some of our galaxies, we explore different interpretations for the excess; namely a disk or halo component.

In the last column of Table 2 we speculate about the nature of the outer light excess with respect to the $r^{1/4}$. The excess has been modeled with an exponential component. The nature of this component depends on several

**Fig. 3.** a) Histogram of the absolute magnitude of the point source; b) Absolute magnitudes of the host galaxies (M_{HOST}) plotted against the absolute magnitudes of the point sources M_{PS} .

factors. Besides the very appearance of the galaxy, one speculation usually relies on different "objective" clues (see also Paper II): a) the central surface brightness of the exponential component, which, in the case of disks, according to Freeman (1970), should span the range 20–20.75 in the R band; b) the c_4 profile, whose positive sign should indicate the presence of a disk component; c) el-

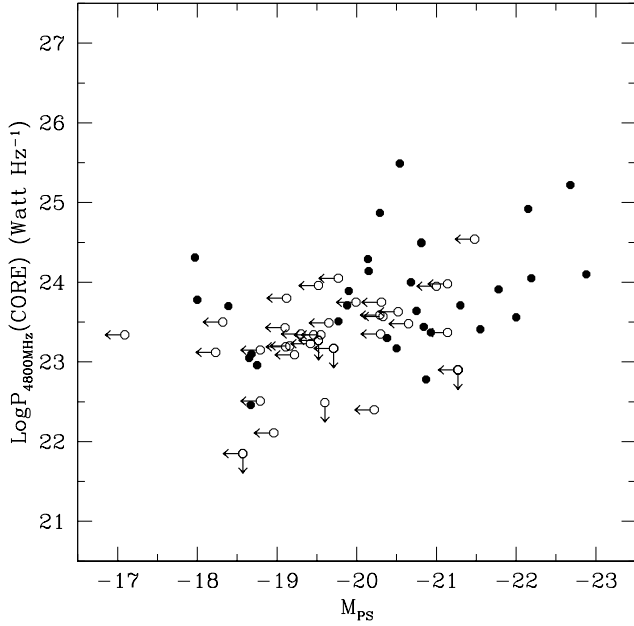


Fig. 4. Relation between core radio power at 4800 MHz and absolute optical magnitude of the point source. Filled circles represent objects with detected optical point sources. Open circles indicate upper limits for the point source contribution or for the core radio power (see text for details).

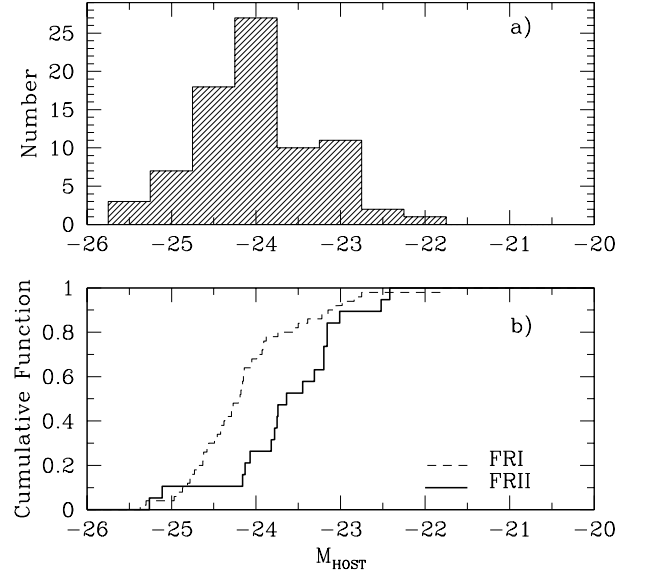


Fig. 6. a) Distribution of absolute total magnitude of the host galaxies in R band. b) Cumulative distribution of the absolute total magnitude of the host galaxies for FRI (dotted line) and FRII (solid line).

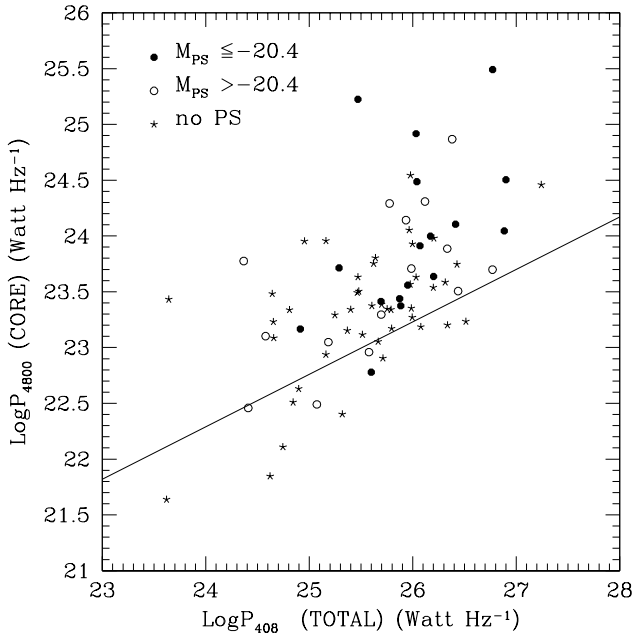


Fig. 5. Relation between total radio power at 408 MHz and core radio power at 4800 MHz. Objects are divided according to luminosity of PS: $M_{PS} < -20.4$ (filled circles), $M_{PS} > -20.4$ (open circles), and undetected PS (stars). The solid line represents the empirical relation found by Giovannini et al. (1988).

liptcities and position angles of the isophotes, which, in the ideal case of thin disks superimposed to ellipsoidal or biaxial bulges, should exhibit increasing or constant ellipticity profiles, respectively. On the basis of these criteria, we found 4 galaxies in which the presence of an outer disk component turns out to be very likely. We also found 11 cases in which the light excesses can be confidently ascribed to the presence of large outer halos. The note "small halo" in Table 2 has been introduced to denote 3 galaxies for which no exponential component has been used in the fit, since the amount of the light excess in the outer region is rather small. Finally, there are 6 cases in Table 2 for which the profile is rather complex and no good fit can be obtained using simple models. In these cases we are not able to decide about the nature of the light excess in the luminosity profiles.

The fraction of galaxies in our sample showing a light excess in the outer profiles is of 25%, a percentage much smaller than that found by Colina & de Juan (1995) (73%). If the excess is attributed to galaxy interactions our results would imply they are significantly less frequent than previously reported and comparable to normal ellipticals.

4. Overall properties of host galaxies

4.1. Absolute magnitudes and effective radii.

We investigate here the optical luminosity and the effective radius of radio galaxies and compare our results with previous findings from other samples of radio galaxies as well as with normal elliptical galaxies.

In Table 5 we report the photometric and structural properties of the observed objects. Column 1 gives the name of the radio galaxy. Column 4 contains the integrated magnitudes of the objects computed within the isophote 24.5. We computed the total magnitudes (column 5) from extrapolation of the surface brightness profiles and we used these values to derive the effective radii R_e (semimajor axis of the isophote enclosing half of the total galaxy light; column 2) and the corresponding effective surface brightness μ_e (column 3). In Table 5 we give the magnitudes and the surface brightness corrected for galactic extinction. The absolute R band magnitudes $M_{HOST}(24.5)$ and $M_{HOST}(tot)$ reported in Table 5 (column 6 and 7) include K-correction (see Paper I-II). Moreover these magnitudes have also been corrected for the contribution of the nuclear component derived from the fit (see Table 5, column 8).

We found that the average absolute magnitude is $\langle M_{HOST}(tot) \rangle = -24.00 \pm 0.69$. The distribution of absolute magnitudes for the whole data-set is presented in Fig. 6a.

We compare our finding on the absolute magnitudes of radio galaxies with the results by Owen & Laing (1989), Smith & Heckman (1989b) and Ledlow & Owen (1995). In order to perform a suitable comparison we have transformed their data to our cosmology. In addition since many authors publish only isophotal magnitudes (at $\mu_R = 24.5$ or $\mu_V = 25$) we applied an average correction of -0.17 mag to transform isophotal magnitudes ($m_{24.5}$) in total magnitudes, an average correction of -0.12 mag to transform isophotal magnitudes (m_{25}) into total magnitudes (these values are taken from our average difference between $m_{24.5}$ and m_{tot} and between m_{25} and m_{tot}). A summary of the comparison of our absolute magnitudes with those from other samples of radio galaxies is given in Table 4, which reports the samples (divided also between FRI and FRII), the mean redshift of the samples, and in brackets, the number of objects in each sample. The agreement between our absolute magnitudes with those from other sample is good. Dividing the radio galaxies according to their radio morphology (FRI and FRII; see previous section) we find that galaxies hosting FRI sources are systematically brighter than those hosting FRII sources. A systematic difference in luminosity between FRI and FRII galaxies was previously suggested by Owen & Laing (1989) from observations of 47 radio galaxies in the R-band.

Including only the objects with good morphological radio classification we found: $\langle M_{HOST}(tot) \rangle_{FRI} = -24.13 \pm 0.69$ and $\langle M_{HOST}(tot) \rangle_{FRII} = -23.62 \pm 0.73$. This dif-

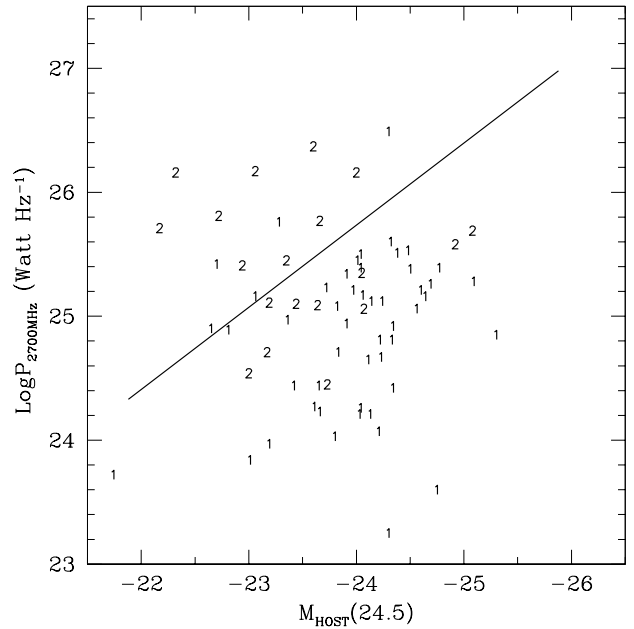


Fig. 7. The radio power at 2700 MHz vs absolute magnitude of the host galaxy. FRI and FRII are indicated as 1 and 2 respectively. The line in the plot represents the segregation between radio power and optical luminosity proposed by Owen & Ledlow (1994).

ference is illustrated in Fig. 6b by comparison of the two cumulative distributions. The Kolmogorov-Smirnov two-samples test yields in this case $P_{KS} = 0.001$.

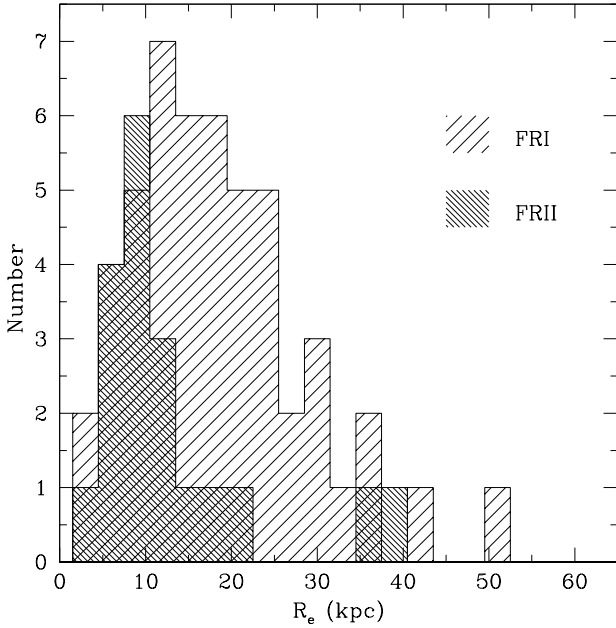
Owen & Laing (1989) and Owen & White (1991) have noted a segregation of FRI and FRII radio galaxies in the radio power to host optical luminosity plane, suggesting that segregation between FRI/FRII sources was not only dependent on the radio power but also on the optical luminosity of the host galaxy. We report in Fig. 7 the total radio luminosity at 2700 MHz versus $M_{HOST}(24.5)$ for our sample. The line in the plot represents the dividing line proposed by Owen & Ledlow (1994) for FRI and FRII.

The scatter of our galaxies over this plane is very large, but the figure suggests that the galaxies associated with different radio morphology (FRI and FRII) fall generally in separate areas of the diagram. A result that, together with the classical radio luminosity division, reflects the difference of average optical galaxy luminosity.

The hosts of FRI radio sources also appear larger than FRII hosts. From our sample we find that the average effective radius is 18.4 ± 10.1 kpc for FRIs and 12.9 ± 9.3 kpc for FRIIs (see Fig. 8). This is likely to be simply a consequence of the relationship between effective radius and luminosity of elliptical galaxies. For our 79 radio galaxies we find:

Table 4. Total absolute R magnitudes of radio galaxies

	This work	Ledlow,Owen	Owen,Laing	Smith,Heckmann
All	−24.00 (79)	-	−23.59 (47)	−23.72 (68)
$\langle z \rangle$	0.053	-	0.081	0.093
FRI	−24.13 (50)	−23.83 (265)	−23.96 (13)	−23.87 (25)
$\langle z_{FRI} \rangle$	0.052	0.087	0.034	0.057
FRII	−23.62 (19)	-	−23.30 (26)	−23.59 (33)
$\langle z_{FRII} \rangle$	0.056	-	0.110	0.123

**Fig. 8.** Effective radius (in kpc) divided between FRI and FRII.

$$M_{HOST} = -20.77(\pm 0.28) - 2.78(\pm 0.24) \times \log(R_e).$$

The same relation appears to apply for normal luminous ellipticals (Romanishin 1986).

4.2. $\mu_e - R_e$ relation

Fig. 9a illustrates the relation $\mu_e - R_e$ (hereafter Kormendy relation; Kormendy 1977) we obtained from our sample of radio galaxies. The effective surface brightnesses of the galaxies have been corrected for galactic extinction and cosmological dimming $10 \times \log(1+z)$. Moreover, effective radii and surface brightnesses of four galaxies with very bright nuclei (2221-02, 0625-35, 0430+05, 0945+07)

have been properly corrected to take into account the contribution of the point source.

The straight line best fitting the whole sample is given by the equation:

$$\mu_e(\text{All}) = 18.44(\pm 0.35) + 2.58(\pm 0.29) \times \log(R_e),$$

which is consistent with the fit obtained in Paper I from our sub-sample of 29 radio galaxies. The fits relative to the FRI and FRII sub-samples are given by:

$$\mu_e(FRI) = 18.51(\pm 0.41) + 2.49(\pm 0.33) \times \log(R_e),$$

$$\mu_e(FRII) = 18.35(\pm 0.61) + 2.71(\pm 0.60) \times \log(R_e).$$

They are represented in Fig. 9a by the full and dotted lines, respectively.

In conclusion, the coefficients of the different $\mu_e - R_e$ relations do not differ significantly from one another.

The effective radii and surface brightnesses in Fig. 9a refer to the isophote enclosing half of the total galaxy light (column 2 of Table 5). We prefer to use these quantities rather than those obtained by fitting the luminosity profiles of the galaxies with a de Vaucouleurs $r^{1/4}$ law because they are model independent. However, since the latter definitions of R_e and μ_e are widely used in the literature, in order to compare our results with those obtained from other samples, we also computed them for our radio galaxies. Fig. 9b illustrates the $\mu_e - R_e^{fit}$ relation from our sample. In this case the best fits to the data turn out to be:

$$\mu_e(\text{All}) = 18.35(\pm 0.24) + 3.00(\pm 0.19) \times \log(R_e)^{fit},$$

$$\mu_e(FRI) = 18.68(\pm 0.26) + 2.70(\pm 0.20) \times \log(R_e)^{fit},$$

$$\mu_e(FRII) = 17.66(\pm 0.69) + 3.71(\pm 0.65) \times \log(R_e)^{fit}.$$

Again the relation relative to the global sample (solid line in Fig. 9b) is fairly consistent with that obtained in Paper I for a much less sizeable sample.

We compared our results with those derived from other samples of radio galaxies. After accounting for the different cosmology, we found a good agreement with the results of Colina & de Juan (1995) for a sample of FRI galaxies ($\mu_e = 18.34 + 3.03 \log(R_e)$) and Smith & Heckman (1989b) for powerful radio galaxies ($\mu_e = 18.22 + 3.03 \log(R_e)$); assuming a color correction $V - R = 0.8$. Instead a signif-

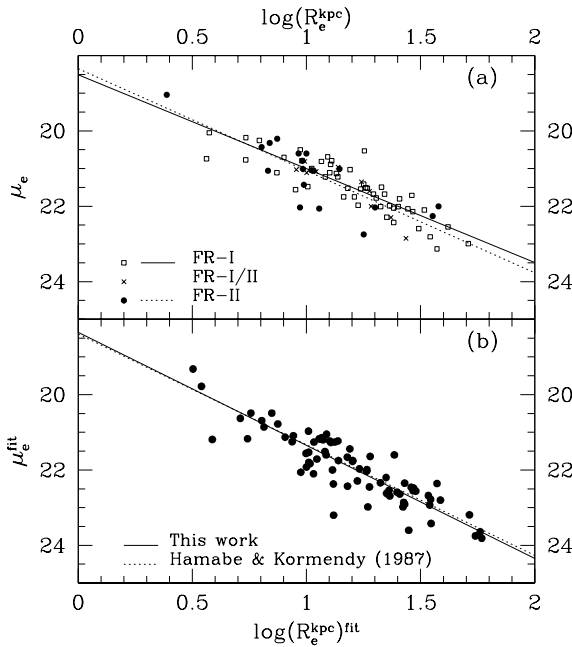


Fig. 9. a) $\mu_e - R_e$ relation. The effective radii and surface brightnesses refer to the isophote enclosing half of the total galaxy light. The solid and dotted lines represent FRI and FRII radio source, respectively; b) $\mu_e - R_e$ relation obtained by fitting with a de Vaucouleurs law the luminosity profile. The solid lines represent the relation relative to the global sample, the dotted lines represent the relation by Hamabe & Kormendy (1987)

icant difference is found with the $\mu_e - R_e$ relation given by Ledlow & Owen (1995) for a sample of FRI galaxies in Abell clusters. They report $\mu_e - R_e$ relationships for various subsamples that systematically differ from ours for brighter zero points and steeper slopes. A possible explanation for this discrepancy is that, at variance with our sample, the Ledlow & Owen galaxies live in rich environments.

It is well known that the Kormendy relation represents the projection on the plane ($\mu_e - R_e$) of the fundamental plane of elliptical galaxies (Djorgovski & Davis 1987, Dressler et al. 1987). This relation has been claimed to be closely related to the morphological and dynamical structure of galaxies, as well as to their formation processes.

It is therefore of interest to compare the Kormendy relation for radio galaxies with that for normal ellipticals. Comparing with the classical $\mu_e - R_e$ relation given by Hamabe & Kormendy (1987) for radio-quiet ellipticals, ($\mu_e = 18.39 + 2.94 \log(R_e)$ in our system); we found the two relationships are indistinguishable (see Fig. 9b).

The fact that the Kormendy relation of radio galaxies is not significantly different from that of normal ellipticals indicates that the formation processes and the structure of galaxies hosting radio sources are similar to those of radio-

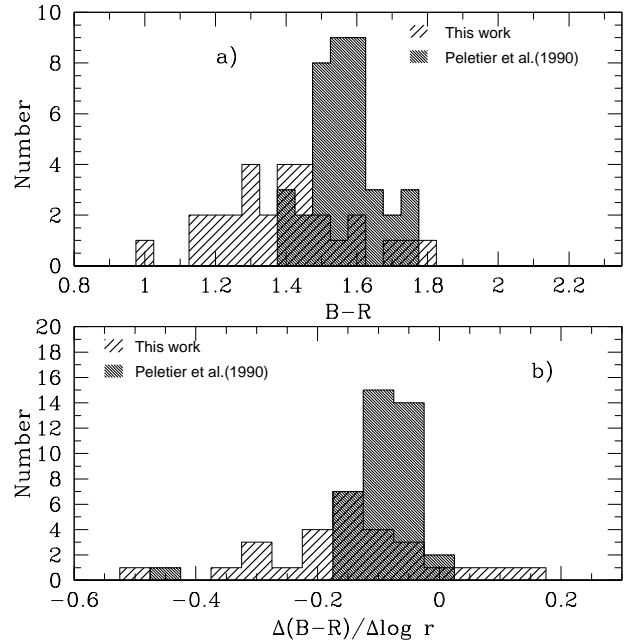


Fig. 10. a) Distribution of the B-R color of radio galaxies compared with normal ellipticals (Peletier et al 1990). b) Distribution of color gradient of radio galaxies (thinly-hatched) compared with normal ellipticals (thickly-hatched).

quiet ellipticals. To go deeper in to this question, we obtained spectroscopic observations of a number of galaxies belonging to our sample, aimed at measuring their velocity dispersions and at investigating the whole fundamental plane of radio galaxies. This analysis is in progress and the results will be reported in a forthcoming paper.

4.3. Colors of the galaxies

For 29 sources in our sample we obtained both B and R images. Photometric and structural profiles for these sources have been reported in Paper I. From these data we derived the integrated colors $B-R$ and the color profiles as a function of the semimajor axis. Colors ($B-R$) in Table 6 (column 2) have been corrected for galactic extinction, k-correction and nuclear component. The distribution of the $B-R$ color is compared in Fig. 10a with that derived from a sample of 39 radio quiet elliptical galaxies (Peletier et al. 1990). It turns out that, the integrated color distribution of radio galaxies is much broader and has a blue tail than elliptical galaxies. In our sample the average integrated color is $\langle B-R \rangle = 1.39 \pm 0.18$ compared with $\langle B-R \rangle = 1.57 \pm 0.09$ of Peletier et al. (1990).

For each object we have also derived the color profile as a function of semi-major axis, combining luminosity profiles in the B and R bands. The color profiles against the logarithmic radius are well represented by a linear fit, but in most objects it appears rather smooth with a sys-

tematic tendency of the galaxies to become bluer in the outer regions.

To quantify this behavior we computed the color gradient $\Delta(B-R)/\Delta \log r$ for each object (see Table 6 column 3) by a linear regression of the color profile.

The mean color gradient is $\langle \Delta(B-R)/\Delta \log r \rangle = -0.16 \pm 0.17$, compared with $\langle \Delta(B-R)/\Delta \log r \rangle = -0.09 \pm 0.07$ for elliptical galaxies of Peletier et al. (1990). The average color gradient in radio galaxies appears therefore slightly steeper than in normal ellipticals while the distribution of color gradient is much broader (see Fig. 10b).

These results on the integrated colors and color gradients are in agreement with the results of Zirbel (1996) who found that on average radio galaxies are bluer by 0.18 mag and have a color dispersion larger than bright cluster member. However, contrary to the finding by Zirbel (1996) we don't find significant difference in the integrated color distribution between FRI and FRII. Also Smith & Heckman (1989) in a study of multicolor surface photometry of powerful radio galaxies, found that in general radio galaxies with strong optical emission line spectra have unusually blue average colors relative to giant elliptical galaxies while radio galaxies with weak or no emission lines have colors and color gradients indistinguishable from those of normal giant ellipticals.

The color variation inside each galaxy and among different galaxies is usually taken to indicate changes in the mean metallicity and/or in the age of the stellar population (Franx & Illingworth 1990). However, the presence of dust could also play a role in the observed color gradient of galaxies (see e.g. Wise & Silva 1996).

The color differences observed could be either intrinsic or due to different dust-reddening for radio galaxies (or a combination of the two effects). The fact that the color profiles are rather smooth and that there is a tendency for the bluer galaxies to have steeper color gradient (see Fig. 11), support the idea that color differences are mostly intrinsic.

As a further comparison concerning the colors of radio galaxies we show in Fig. 12 the color-magnitude relation of our sample compared with standard color-magnitudes relations for elliptical galaxies (Peletier et al. 1990; Lopez-Cruz 1997). It turns out clearly that radio galaxies systematically deviate from the standard color-magnitude relationship even if some of the brightest non-radio ellipticals cover the same region of the radio galaxies. A possible suggestion is that the color-magnitude relationship undergoes a breakdown at the highest luminosities.

5. Structural and morphological properties

5.1. Ellipticity

The distribution of the observed ellipticity ϵ in a sample of elliptical galaxies gives interesting information about

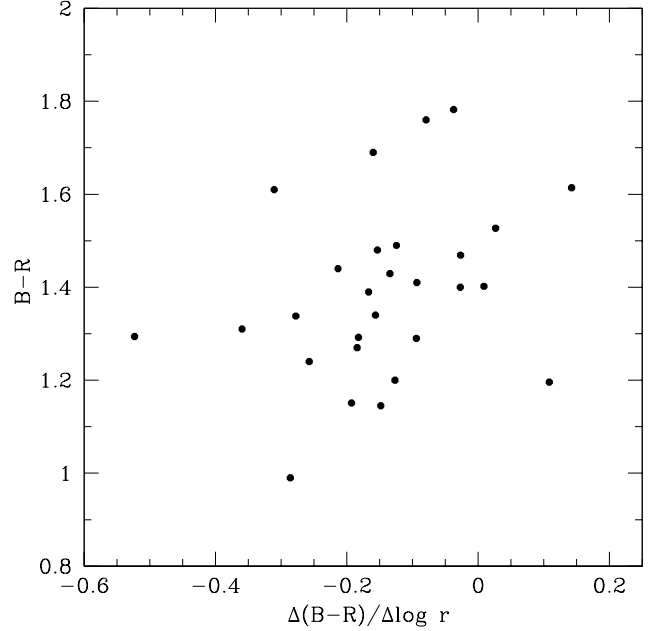


Fig. 11. Relation between B-R color and color gradient of our radio galaxies

the intrinsic shapes of the galaxy population. Introducing some "a priori" hypothesis on the geometrical properties of the galaxy body (oblate, prolate, triaxial), one can deproject the observed ellipticity distribution to infer the distribution of the intrinsic ellipticities. In practice, even if deprojecting ellipticity distributions is an ill-posed problem (generally it has no unique solution), a significant difference between the observed distributions of two galaxy populations implies a difference in their intrinsic shape.

From surface photometry analysis we obtained for each object the ellipticity profile. In order to characterize the ellipticity of the galaxies we took the values of ϵ at the effective radius (see column 9 in Table 5).

From our sample we find $\langle \epsilon_e \rangle = 0.21 \pm 0.12$, while the mean ellipticity at $\mu_R = 24.5$ is $\langle \epsilon_{24.5} \rangle = 0.25 \pm 0.12$. Considering the two subsamples of FRI and FRII we did not find any significant difference ($P_{KS} = 0.52$) between the two populations:

$$\begin{aligned} \langle \epsilon_e \rangle_{FRI} &= 0.21 \pm 0.11 \\ \langle \epsilon_e \rangle_{FRII} &= 0.21 \pm 0.12. \end{aligned}$$

The distribution of ϵ_e from our sample is shown in Fig. 13a. We compared this distribution with the corresponding one from a large data-set of normal ellipticals by Fasano & Vio (1991) (Fig. 13b). It is found that both distributions are peaked around 0.2. The KS test (Fig. 13c) shows that the two data sets are likely to be drawn from the same parent population ($P_{KS} = 0.97$).

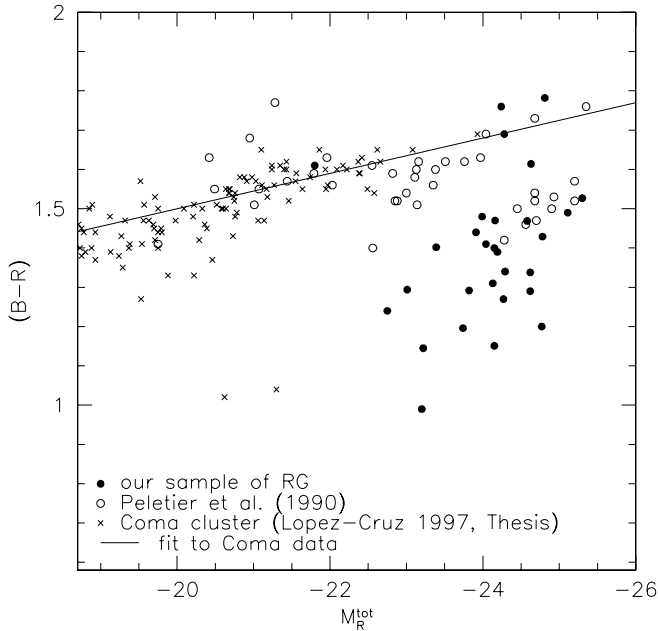


Fig. 12. Color-magnitude relation of our sample compared with standard color-magnitude relations for elliptical galaxies (Peletier et al. 1990; Lopez-Cruz 1997)

This result is at variance with the suggestion by Disney et al. (1984), and Calvani et al. (1989), that radio galaxies tend to be rounder than radio-quiet ellipticals.

Our result confirms the previous finding of Smith & Heckman (1989b) that powerful radio galaxies have identical ellipticity distribution of non radio ellipticals. They argued that the difference noted by Disney et al. (1984) may be due to different radio power of the galaxies considered.

Again, no difference in ellipticity between radio galaxies and radio-quiet ellipticals was found by Ledlow & Owen (1995) comparing the distribution of $\epsilon_{24.5}$ from a sample of radio galaxies (FRI) in clusters with that relative to a control sample of normal galaxies in the same environment.

It is noticeable that even the host galaxies of quasars appear to exhibit the same ellipticity distribution of normal galaxies (McLure et al. 1999) supporting the idea that this morphological parameter is very little (if not at all) influenced by nuclear activity.

5.2. Isophote shape: *disky* and *boxy*

If the residual intensity variations along a best fitting ellipse are expanded as a Fourier series in the azimuthal angle θ , the coefficient c_4 , associated with the $\cos(4\theta)$ term is found to have a relatively large amplitude. The amplitude of the c_4 parameter, indicates deviations of the isophote shape from perfect ellipse in the form of *disky* isophotes

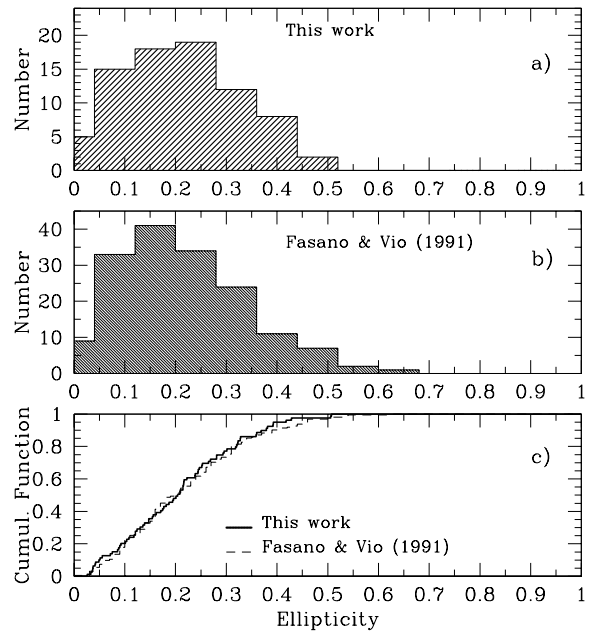


Fig. 13. a) Distribution of ellipticity calculated at the effective radius. b) Distribution of ellipticity in a sample of non radio ellipticals (Fasano & Vio 1991). Panel c) shows the comparison of the two cumulative distributions.

($c_4 > 0$) or *boxy* isophotes ($c_4 < 0$). We have examined the radial profile of c_4 and evaluated the global amplitude of the c_4 parameter using two different methods. In the first one we calculated the value of c_4 at the effective radius, in the second one we derived for each galaxy a weighted average value of c_4 over the profile. The two different methods give similar results. Therefore in the following we will use the percentage value of c_4 at the effective radius (Table 5, column 12).

In Fig. 14a we show the distribution of c_4 from our sample of radio galaxies. We find that about 50% of our objects are *boxy* and 50% are *disky*. Moreover the distributions of c_4 taken for the sample of FRI and FRII galaxies are essentially the same. Finally there is no correlation between radio power and shape of isophotes (see Fig. 14b).

This is in contrast with the results by Bender et al. (1987) who found a correlation between isophote shape and radio emission in elliptical galaxies in the sense that radio-loud objects have generally *boxy* or irregular isophotes. On the other hand, two more studies concerning the morphology of radio galaxies support our conclusion. First, the fraction of *boxy* ellipticals found by Gonzalez-Serrano et al. (1993) in radio galaxies is significantly lower than that reported by Bender et al. (1987). Second, the radio galaxies in Abell cluster studied by Ledlow & Owen (1995), do not show an higher percentage of *boxy* isophotes with respect to a control sample of radio-quiet ellipticals.

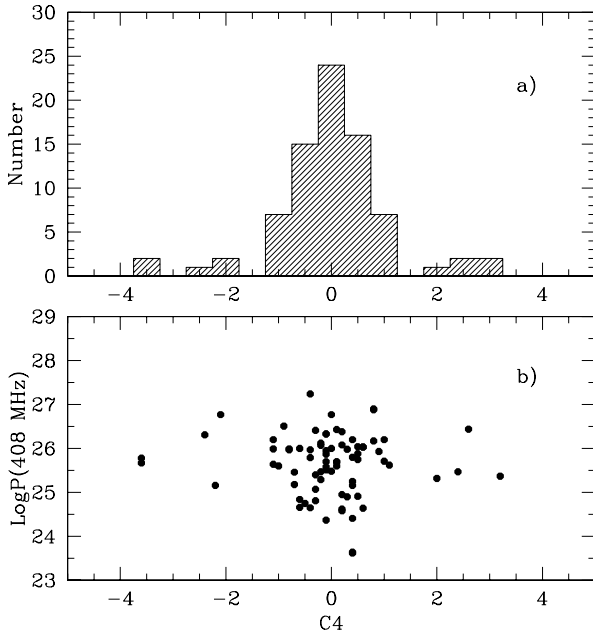


Fig. 14. a) Histogram of the c4 parameter for our sample of radio galaxies; b) Radio power at 408 MHz versus the c4 parameter.

6. Signature of interaction

The isophotal analysis of the host galaxies is important to understand whether or not there are signatures of gravitational interaction. These signatures include isophote twisting, non-concentric isophotes and/or the presence of close companions with signs of a disturbed morphology. In this section characteristic values for these morphological distortions are evaluated and compared with the corresponding values taken from other samples of both radio and non radio ellipticals.

6.1. Non concentric isophotes

The presence of non concentric isophotes is among the strongest evidences of interaction between members of galaxy pairs or groups. We quantify the presence of non concentric isophotes by the parameter $\delta = \Delta R/R$ where $\Delta R = [(X_c - X_o)^2 + (Y_c - Y_o)^2]^{1/2}$. It represents the percentage of displacement of the isophotes with respect to the size of the galaxy. X_o and Y_o represent the position of the center of the inner isophotes, while R is the radius of the isophote, having X_c and Y_c as center coordinates. Since δ may slightly change with R we took the value at the effective radius R_e . In Fig. 15 we show the histogram of the δ parameter. The average value of δ for the whole sample is 0.03 with no significant difference between galaxies hosting FRI and FRII radio sources.

Apparent isophote displacement could be induced by the photometric superposition of two galaxies as in the

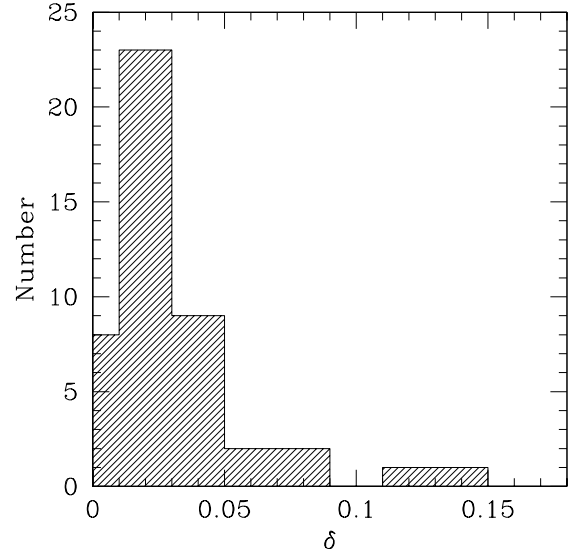


Fig. 15. Distribution of the δ parameter

case of Dumbbell systems. Therefore for objects with large close companions we have adopted a two recursive fitting analysis (see Paper I). It turned out that in most cases no significant displacement of isophotes is present in the two galaxies.

In a sample of 44 FRI radio galaxies studied by Colina & De Juan (1995), the average value of δ is 0.05. Comparing their result with those of 40 normal elliptical galaxies studied by Sparks et al. (1991) ($\langle\delta\rangle = 0.017$), they concluded that FRI host galaxies are more widely distributed over δ and show much larger values of δ than non radio ellipticals. Our result, lies between the previous two and suggests again that the role of interactions for radio galaxies is less relevant than previously believed.

6.2. Isophotal Twisting

Isophotal twisting is indicated by the position angle variation of the ellipse's major axis as a function of radius. Kormendy (1982) showed that significant twists are found preferentially in galaxies with prominent companions rather than in nearly isolated galaxies, suggesting that tidal effects may account for most large twists detected to date. On the other hand, Fasano & Bonoli (1989) found the amount of isophotal twisting in their sample of 43 isolated ellipticals to be similar to that detected in randomly selected samples. They concluded that most of the twisting observed in elliptical galaxies is intrinsic (triaxiality).

However, it is worth noting that two other factors may produce apparent isophotal twisting: the overlapping with isophotes of nearby projected companions, a residual gra-

Table 5. Photometric and structural parameters of radio galaxies.

IAU name (1)	R_e (kpc) (2)	μ_e (3)	$m_{24.5}$ (4)	m_{tot} (5)	$M_{HOST}(24.5)$ (6)	$M_{HOST}(tot)$ (7)	M_{PS} (8)	ϵ_e (9)	ΔPA (10)	δ (11)	c4 (12)
0005 – 199	25.2	22.51	15.15	14.95	–24.38	–24.58	–20.68	0.33	3.8	0.041	0.8
0013 – 316	34.8	23.25	14.98	14.62	–24.24	–24.62	–20.84	0.21	15.7	0.029	–0.1
0023 – 333	51.1	23.20	13.16	12.88	–24.34	–24.62	...	0.38	5.2	0.034	–3.6
0034 – 014	10.0	21.42	14.72	14.58	–23.6	–23.74	–20.29	0.04	9.3	...	0.2
0055 – 016	12.7	21.30	13.22	13.11	–24.04	–24.15	...	0.03	10.2	0.023	0
0123 – 016	18.9	21.68	11.33	11.16	–23.87	–24.04	< –18.8	0.36	5.9	...	3.2
0131 – 367	14.0	21.14	12.29	12.18	–24.05	–24.16	...	0.30	39.4	0.056	3.1
0229 – 208	13.7	21.59	14.82	14.64	–24.01	–24.19	< –21.5	0.14	0.3
0247 – 207	32.9	22.46	13.63	13.43	–25.09	–25.3	–21.78	0.12	22.5	0.039	–0.2
0255 + 058	5.4	20.87	12.92	12.75	–22.81	–22.98	–18.75	0.03	22.8	0.015	–0.1
0257 – 398	7.4	20.49	14.48	14.38	–23.64	–23.74	< –21.3	0.21	11.9	0.012	1.0
0307 – 305	9.6	21.29	14.81	14.70	–23.19	–23.31	–20.87	0.30	7.8	0.048	–1.0
0312 – 343	22.5	22.57	14.22	14.01	–23.83	–24.06	–21.3	0.20	3.1	0.026	–0.2
0325 + 023	20.0	22.16	12.90	12.70	–23.44	–23.64	< –19.1	0.39	3	0.015	–1.1
0332 – 391	12.1	21.49	14.21	14.06	–23.72	–23.88	–20.93	0.18	9.6	...	0.5
0344 – 345	9.0	21.78	14.83	14.70	–22.7	–22.84	–19.88	0.21	5.8	0.023	–0.8
0349 – 278	17.8	23.03	15.34	15.06	–22.72	–23.01	–19.77	0.32	10.4	...	2.6
0427 – 539	20.2	21.94	12.82	12.69	–24.04	–24.17	< –20.3	0.33	9.8	...	–0.8
0430 + 052	7.4	21.25	13.07	13.01	–23.06	–23.15	–22.68	0.09	13	0.038	2.4
0434 – 225	27.8	22.36	13.56	13.33	–24.64	–24.87	–20.38	0.10	20.1	0.035	0.1
0446 – 206	10.1	21.79	14.99	14.81	–23.36	–23.54	< –19.3	0.05	16	0.009	0.5
0449 – 175	14.5	21.88	12.76	12.50	–23.65	–23.91	...	0.17	7.8	...	0.3
0452 – 190	16.8	22.14	13.26	13.00	–23.66	–23.92	...	0.21	7.9	0.001	–0.4
0453 – 206	19.2	22.15	12.75	12.57	–23.93	–24.11	< –19.5	0.10	17.5	0.027	–0.4
0511 – 305	11.4	22.30	14.88	14.66	–22.94	–23.16	< –19.1	0.12	21.4	...	0.2
0533 – 377	24.1	22.83	14.85	14.57	–24.14	–24.42	< –20.0	0.12	17.7	0.019	1.1
0546 – 329	18.5	21.68	12.46	12.34	–24.34	–24.46	...	0.20	3.1	0.015	0.4
0548 – 317	9.7	21.58	13.57	13.42	–23	–23.16	–19.6	0.24	4.1	0.011	–0.3
0620 – 526	28.9	21.93	12.73	12.53	–24.77	–24.97	–20.81	0.25	8.5	...	0.5
0625 – 354	19.6	21.91	13.27	13.11	–24.32	–24.49	–22.15	0.22	6.7	...	0.6
0625 – 536	37.9	22.23	12.57	12.39	–25.08	–25.26	< –20.3	0.37	8.7	0.136	0.1
0634 – 205	9.8	21.05	14.10	13.90	–23.64	–23.84	< –19.4	0.18	28.9	...	–0.9
0712 – 349	11.6	21.00	13.15	12.98	–24.04	–24.21	< –19.5	0.16	3.8	0.01	–0.3
0718 – 340	11.0	21.20	12.35	12.15	–23.9	–24.1	–18.65	0.12	19.8	...	–0.7
0806 – 103	10.0	21.05	15.27	15.20	–24	–24.07	–20.81	0.09	32.9	...	0.8
0915 – 118	22.0	21.91	13.35	13.23	–24.3	–24.42	...	0.19	8.4	...	–0.4
0940 – 304	9.4	20.66	13.25	13.12	–23.61	–23.74	< –20.6	0.42	7.2	0.023	0.6
0945 + 076	6.8	21.42	15.29	15.19	–23.06	–23.2	–22.19	0.04	2.8	0.015	0.8
1002 – 320	21.1	22.38	14.75	14.52	–24.06	–24.29	< –19.5	0.20	16.2	0.024	–0.6
1043 – 290	37.4	23.38	13.68	13.22	–24.22	–24.68	< –19.5	0.09	9.5	...	–2.2
1053 – 282	29.2	22.40	13.99	13.86	–23.91	–24.05	–20.14	0.51	4.4	...	–3.6
1056 – 360	9.0	21.32	14.84	14.64	–23.41	–23.61	< –19.8	0.13	52.1	0.009	–0.4
1107 – 372	12.4	20.73	9.61	9.53	–24.3	–24.38	...	0.26	5.7	0.006	0.4
1123 – 351	24.1	22.19	12.15	11.92	–24.33	–24.56	< –18.3	0.15	5.3	0.019	0
1251 – 122	12.91	20.85	10.70	10.63	–24.11	–24.18	...	0.32	6.5	0.122	0.4
1251 – 289	17.9	20.77	12.48	12.41	–25.3	–25.37	< –19.7	0.05	70.3	0.086	0.4
1257 – 253	15.2	21.79	14.17	13.92	–23.91	–24.16	< –19.6	0.25	5.1	0.004	–0.7
1258 – 321	17.3	21.61	10.87	10.71	–24.21	–24.37	–18.68	0.22	5.4	0.016	0.2
1318 – 434	18.1	21.56	10.09	9.98	–24.03	–24.14	...	0.28	13.6	...	–0.3
1323 – 271	17.4	21.54	13.22	13.14	–23.97	–24.05	< –18.2	0.51	4.5	0.032	–0.1
1333 – 337	13.8	21.02	10.05	9.97	–24.43	–24.52	< –17.1	0.09	29.2	0.004	–0.3
1344 – 241	6.2	20.34	12.43	12.37	–23.01	–23.07	< –18.6	0.43	2	0.018	0.2
1354 – 251	9.5	20.95	13.44	13.36	–23.42	–23.5	< –18.8	0.39	5.8	0.011	–0.6

Table 5 (continued). Photometric and structural parameters of radio galaxies.

IAU name (1)	R_e (kpc) (2)	μ_e (3)	$m_{24.5}$ (4)	m_{tot} (5)	$M_{HOST}(24.5)$ (6)	$M_{HOST}(tot)$ (7)	M_{PS} (8)	ϵ_e (9)	ΔPA (10)	δ (11)	c4 (12)
1400 – 337	25.6	21.86	9.89	9.72	–24.75	–24.92	< –19.0	0.22	17.3	0.012	–0.5
1404 – 267	16.2	21.84	11.84	11.71	–23.8	–23.93	–18	0.19	6.7	0.017	–0.1
1514 + 072	41.6	22.70	12.06	11.81	–24.56	–24.81	–17.97	0.36	3	0.038	–0.2
1521 – 300	3.6	20.83	13.70	13.64	–21.74	–21.8	< –19.1	0.24	11.6	0.061	0.4
1637 – 771	6.9	20.49	13.64	13.54	–23.35	–23.45	–20.15	0.32	33.9	...	0.9
1717 – 009	9.4	22.16	14.07	13.87	–22.32	–22.52	–18.39	0.04	35	0.01	0
1733 – 565	10.8	21.47	15.39	15.22	–23.6	–23.78	–20.54	0.21	18	0.029	–2.1
1928 – 340	21.3	21.90	14.44	14.31	–24.6	–24.73	< –21.1	0.14	5	...	–1.1
1929 – 397	35.7	22.57	13.44	13.25	–24.92	–25.11	...	0.24	23.6	...	1.0
1949 + 023	9.2	20.85	14.20	14.11	–23.66	–23.75	< –19.2	0.25	16.3	...	–0.1
1954 – 552	8.0	20.94	14.50	14.40	–23.28	–23.39	–19.9	0.24	4.8	...	–0.1
2013 – 308	15.5	21.40	14.03	13.95	–24.69	–24.78	–22	0.17	37.6	...	–0.1
2031 – 359	23.1	22.36	14.28	14.14	–24.48	–24.63	–20.75	0.15	18	...	0.4
2040 – 267	9.6	20.96	12.97	12.91	–24.07	–24.13	< –21.1	0.03	25.5	...	0.1
2058 – 282	27.3	23.02	12.94	12.65	–23.99	–24.28	...	0.07	11	...	0.6
2059 – 311	17.8	21.58	12.80	12.66	–24.13	–24.27	< –19.2	0.38	1.5	...	–0.6
2104 – 256	23.4	22.46	12.97	12.63	–23.9	–24.24	< –20.3	0.27	8	...	–2.4
2128 – 388	5.4	20.26	12.00	11.97	–23.19	–23.22	–18.67	0.16	4.5	0.027	0.4
2158 – 380	6.4	20.58	13.44	13.41	–23.17	–23.2	< –20.2	0.28	12.3	...	2.0
2209 – 255	12.8	21.16	13.78	13.72	–24.23	–24.29	< –21.0	0.32	4.6	...	0.2
2221 – 023	2.4	19.28	14.56	14.46	–22.17	–22.42	–22.88	0.04	7.5	0.028	–0.3
2225 – 308	3.7	20.29	15.10	15.00	–22.65	–22.75	< –20.5	0.07	12.4	...	–0.2
2236 – 176	31.0	22.88	13.76	13.49	–24.5	–24.77	< –20.3	0.11	34.2	...	–1.1
2333 – 327	10.5	21.26	13.79	13.71	–23.73	–23.82	–20.5	0.15	15.5	0.037	0.5
2350 – 375	13.5	21.61	15.38	15.21	–23.97	–24.15	–21.55	0.29	18.5	...	0.1
2353 – 184	10.5	21.31	14.55	14.38	–23.82	–23.99	...	0.05	19.6	0.073	–0.1

dient of the background. These factors could lead to different results in the position angle estimates, depending on the different image quality, on the image processing used and on the criteria used to define a twist as significant. A characteristic of the isophotal twist is that it correlates with the ellipticity, in the sense that the roundest galaxies show the largest twists (Galletta 1980), while very elongated systems show small twists.

We give a measure of the isophotal twist in Table 5 (column 10). The measurement represents the maximum absolute twist over the range of the observed isophotes. When computing the maximum absolute twist, because of the seeing effects, we excluded the isophotes having radii less than $5''$ and the values of PA having errors larger than 8° .

In Fig. 16 we plot the twisting (ΔPA) versus the ellipticity at the effective radius for our sample of radio galaxies. The typical tendency for rounder radio galaxies to show larger twist is confirmed.

In Fig. 17a we plot the distribution of ΔPA from our sample. The average value of ΔPA is $\simeq 14^\circ \pm 12$ (median $\simeq 10^\circ$). We find no difference in twisting between galaxies

hosting different kinds of radio sources: $\langle \Delta PA(FRI) \rangle = 13^\circ \pm 12$, $\langle \Delta PA(FRII) \rangle = 15^\circ \pm 12$.

Compared with the finding of Fasano & Bonoli (1989): $\Delta PA \simeq 21^\circ \pm 16$ (median $\simeq 16^\circ$) for a sample of 43 isolated elliptical galaxies (see Fig. 17b) we don't find any indication that radio galaxies exhibit larger isophote twisting than normal ellipticals. Since we used the same method to derive ΔPA no systematic effects due to different analysis are present.

On the other hand this result contrasts with Colina & de Juan (1995) that, for a sample of 44 FRI radio galaxies, found a larger twisting ($\Delta PA \simeq 30^\circ$; median $\sim 14^\circ$) with respect to the Sparks et al. (1991) sample of normal ellipticals ($\Delta PA \simeq 10^\circ$; median $\sim 4^\circ$).

7. Summary and conclusions

We have presented the results of the analysis of R band imaging for 79 low redshift radio galaxies. These were extracted from two flux-limited samples of radio sources and include objects of both FRI and FRII morphology in the radio power range from 1.8×10^{23} to 3.1×10^{26} Watt/Hz. For these objects we are able to investigate the optical properties of the host galaxies and study their relation-

Table 6. Color index and color gradients

IAU name (1)	(B-R) (2)	$\Delta(B-R)/\Delta\log r$ (3)
0005 – 199	1.47	−0.027
0013 – 316	1.34	−0.278
0023 – 333	1.29	−0.094
0034 – 014	1.20	0.108
0055 – 016	1.4	−0.027
0123 – 016	1.41	−0.093
0131 – 367	1.47	−0.677
0229 – 208	1.39	−0.167
0247 – 207	1.53	0.027
0349 – 278	1.29	−0.523
0449 – 175	1.44	−0.213
1514 + 072	1.78	−0.037
1521 – 300	1.61	−0.311
1929 – 397	1.49	−0.124
1954 – 552	1.40	0.009
2013 – 308	1.43	−0.134
2031 – 359	1.61	0.142
2040 – 267	1.31	−0.360
2058 – 282	1.69	−0.160
2059 – 311	1.27	−0.184
2104 – 256	1.76	−0.079
2128 – 388	1.14	−0.148
2158 – 380	0.99	−0.286
2209 – 255	1.34	−0.156
2225 – 308	1.24	−0.257
2236 – 176	1.2	−0.127
2333 – 327	1.29	−0.182
2350 – 375	1.15	−0.193
2353 – 184	1.48	−0.153

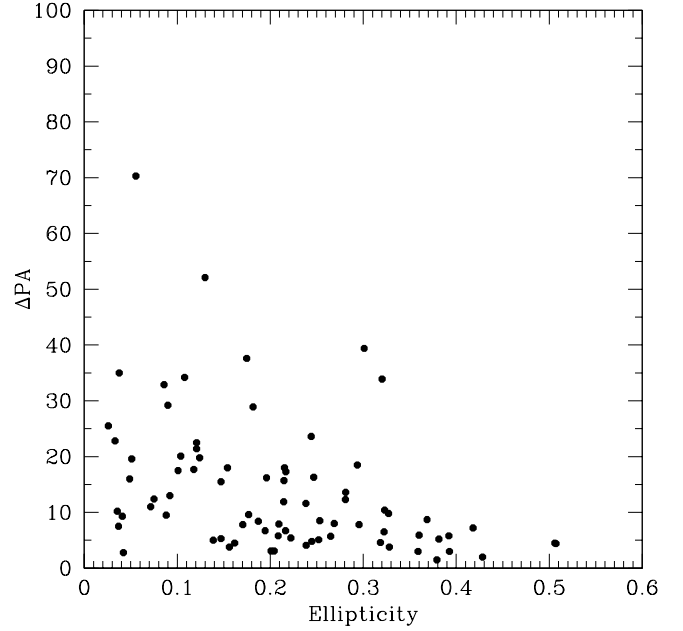
ship with the radio properties. The main results of this study can be summarized as follows:

1) Galaxies are bulge dominated systems with average absolute magnitude $\langle M_{HOST}(tot) \rangle = -24.0$; FRI sources are hosted in galaxies ~ 0.5 mag more luminous than FR II galaxies.

2) Apart from the different average luminosity and size there are not other significant structural differences between galaxies hosting FRI and those hosting FR II radio sources.

3) A substantial fraction ($\sim 40\%$) of the objects observed show the presence of nuclear point sources whose luminosity is about few percent that of the whole galaxy; the luminosity of this component appears correlated with the core radio power but independent of the luminosity of the host galaxy.

4) Several objects ($\sim 40\%$) exhibit deviations of the luminosity profiles with respect to the $r^{1/4}$ law; these deviations appear either as lack of light in the inner ($r < 2$ kpc) region or as light excess in the outer region ($r > 10$ kpc)

**Fig. 16.** Plot of the twisting (ΔPA) versus ellipticity at the effective radius for our sample of radio galaxies.

5) Ellipticity distribution of radio galaxies is indistinguishable from that of normal ellipticals while isophote twisting and de-centering of isophotes are comparable with that found in normal ellipticals.

6) Deviations of isophote from ellipses (disky vs boxy) are in general rather small and show a homogeneous distribution with no preference for disk or boxy isophote shape; no correlation is found between radio power and boxiness of isophotes as suggested by previous studies.

7) Radio galaxies have bluer integrated colors ($B - R$) than normal ellipticals and the color gradients are systematically steeper indicating a slightly bluer population in the outer region with respect to (non-radio) elliptical. Radio galaxies appear to deviate significantly from color-magnitude relation found for normal early type galaxies.

Apart from the difference in the colors these results indicate that in general galaxies hosting radio sources have the same structure and properties as radio-quiet ellipticals. The main distinguishing feature is the presence of nuclear point sources as found in several objects. Our results support the idea that all massive ellipticals may become radio loud at some time and that the radio activity phenomenon does not change significantly the structural and photometric properties of the host galaxies. The color differences, if due to intrinsic differences of stellar population, suggest that the star formation rate may have been increased by the activity phenomenon.

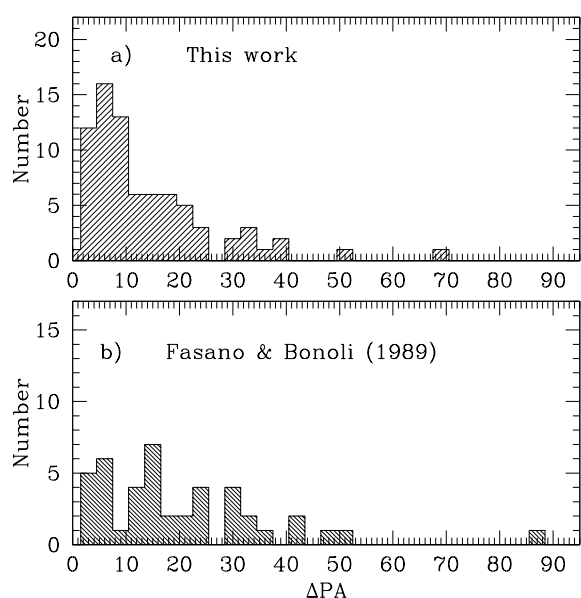


Fig. 17. a) Distribution of ΔPA for our sample. b) Distribution of ΔPA studied by Fasano & Bonoli (1989) for a sample of 43 isolated elliptical galaxies.

Acknowledgments

This work was partly supported by the Italian Ministry for University and Research (MURST) under grant Cofin98-02-32. This research has made use of the NASA/IPAC Extragalactic Database (NED) which is operated by the Jet Propulsion Laboratory, California Institute of Technology, under contract with the National Aeronautics and Space Administration.

References

- Bender R., Döbereiner S., Möllenhoff C., 1987, *A&A* 177, L53
 Calvani M., Fasano G., Franceschini A., 1989, *AJ* 97, 1319
 Capetti A., Celotti A., 1999, *MNRAS* 304, 434
 Chiaberge M., Capetti A., Celotti A., 1999, *A&A* 349, 77
 Colina L., de Juan L., 1995, *ApJ* 448, 548
 Colina L., Perez-Fournon I., 1990, *ApJ* 349, 45
 de Juan L., Colina L., Perez-Fournon I., 1994, *ApJS* 91, 507
 de Vaucouleurs G., 1948, *Ann. Astrophys.* 11, 247
 Disney M.J., Sparks W.B., Wall J.V., 1984, *MNRAS* 206, 899
 Djorgovski S., Davis M., 1987, *ApJ* 313, 59
 Dressler A., Lynden-Bell D., Burstein D., et al., 1987, *ApJ* 313, 42
 Ekers R.D., Wall J.V., Shaver P.A., et al., 1989, *MNRAS* 236, 737 (EK)
 Falomo R., Urry C.M., Scarpa R., Pesce J.E., Treves A., 1999, in *BL Lac phenomenon*, ASP Conference Series, Vol. 159, p. 389, ed. L.O. Takalo, A. Sillanpää
 Fanaroff B.L., Riley J.M., 1974, *MNRAS* 167, 31P
 Fanti R., 1984, in *Clusters and Groups of Galaxies*, edited by F. Mardirossian, G. Giuricin, M. Mezzetti (Reidel, Dordrecht), p. 185
 Fasano G., 1990, internal report of Astr. Obs. of Padova
 Fasano G., Bonoli C., 1989, *A&AS* 79, 291
 Fasano G., Bonoli C., 1990, *A&A* 234, 89
 Fasano G., Vio R., 1991, *MNRAS* 249, 629
 Fasano G., Falomo R., Scarpa R., 1996, *MNRAS* 282, 40
 Franx M., Illingworth G., 1990, *ApJ* 359, L41
 Freeman K.C., 1970, *ApJ* 160, 811
 Galletta G., 1980, *A&A* 81, 179
 Giovannini G., Feretti L., Gregorini L., Parma P., 1988, *A&A* 199, 73
 Giovannini G., Feretti L., Venturi T., Lara L., et al., 1994, *ApJ* 435, 116
 Gonzalez-Serrano J.I., Carballo R., Perez-Fournon I., 1993, *AJ* 105, 1710
 Govoni F., Falomo R., Fasano G., Scarpa R., 1999, *A&AS*, submitted
 Hamabe M., Kormendy J., 1987, in *Structure and Dynamics of Elliptical Galaxies*, IAU Symp. N. 127, p.379, ed. de Zeeuw, Reidel, Dordrecht.
 Hill G.J., Lilly S.J., 1991, *ApJ* 367, 1
 Hine R.G., Longair M.S., 1979, *MNRAS* 188, 111
 Jones P.A., Mc Adam W.B., 1992, *ApJS* 80, 137
 Kleijn G.A., Baum S.A., de Zeeuw P.T., O'Dea C.P., 1999, Submitted to *AJ*, astro-ph/9909256
 Kormendy J., 1977, *ApJ* 218, 333
 Kormendy J., 1982, in *Morphology and Dynamics of Galaxies*, 12th Advanced Course of the Swiss Society of Astronomy and Astrophysics, ed. L. Martinet, M. Mayor, p. 113
 Ledlow M.J., Owen F.N., 1995, *AJ* 109, 853
 Lilly S.J., Prestage R.M., 1987, *MNRAS* 225, 531
 Longair M.S., Seldner M., 1979, *MNRAS* 189, 433
 Lopez-Cruz O., 1997, Ph.D Thesis
 McLure R.J., Dunlop J.S., Kukula M.J., et al., 1999, *MNRAS* 308, 377
 Morganti R., Killeen N.E.B., Tadhunter C.N., 1993, *MNRAS* 263, 1023
 Morganti R., Oosterloo T.A., Reynolds C.N., Tadhunter C.N., Migenes V., 1997, *MNRAS* 284, 541
 Owen F.N., Laing R.A., 1989, *MNRAS* 238, 357
 Owen F.N., Ledlow M.J., 1994, in *The First Stromlo Symposium: The Physics of Active Galaxies*, ASP Conference Series, Vol. 54, p.319, ed. G.V. Bicknell, M.A. Dopita, P.J. Quinn
 Owen F.N., White R.A., 1991, *MNRAS* 249, 164
 Peletier R.F., Davies R.L., Illingworth G.D., Davis L.E., Cawson M., 1990, *AJ* 100, 1991
 Pentericci L., Röttgering H.J., Miley G.K., et al., 1999, *A&A* 341, 329
 Prestage R.M., Peacock J.A., 1988, *MNRAS* 230, 131
 Romanishin W., 1986, *AJ* 91, 76
 Sersic J.L., 1968, *Atlas de Galaxias Australes*, Observatorio Astronomico, Cordoba
 Smith E.P., Heckman T.M., 1989a, *ApJS* 69, 365
 Smith E.P., Heckman T.M., 1989b, *ApJ* 341, 658
 Sparks W.B., Wall J.V., Jorden P.R., Thorne D.J., van Breda I., 1991, *ApJS* 76, 471
 Wall J.V., Peacock J.A., 1985, *MNRAS* 216, 173 (WP)
 Wise M.W., Silva D.R., 1996, *ApJ* 461, 155
 Wise M.W., Silva D.R., 1997, *The Nature of Elliptical Galaxies; 2nd Stromlo Symposium*, ASP Conference Series, Vol. 116, p. 364, ed. M. Arnaboldi, G.S. Da Costa, P. Saha
 Zirbel E.L., 1996, *ApJ* 473, 713